The Journal of Neuroscience, August 1994, 14(8): 5011–5027

ω-Conotoxin Block of N-Type Calcium Channels in Frog and Rat Sympathetic Neurons

Linda M. Boland, James A. Morrill, and Bruce P. Bean

Department of Neurobiology, Harvard Medical School, Boston, Massachusetts 02115

Block of N-type Ca channels by ω-conotoxin GVIA (CgTx) was studied in freshly dissociated bullfrog and rat sympathetic neurons. With 2–5 mM Ba as charge carrier, CgTx blocked almost all of the high-threshold Ca channel current recorded in the presence of nimodipine (3 μM) to block L-type Ca channels. Toxin block reversed slowly (time constant ~ 1 hr) in frog cells and even more slowly in rat cells. CgTx block was faster and more potent in rat cells than frog cells. The rate of block was proportional to CgTx concentration, consistent with 1:1 binding of CgTx to channels. When the external Ba concentration was increased, the development of block was slower, consistent with competition between CgTx and Ba for a binding site. The recovery from block was somewhat faster in higher external Ba. Some cells had significant current remaining in saturating concentrations of nimodipine and CgTx, especially with high Ba concentrations in the external solution. The current resistant to nimodipine and CgTx was activated at lower depolarizations than the CgTx-sensitive current and had faster activation and inactivation kinetics, but unlike low-threshold T-type current, the resistant current had rapidly decaying tail currents.

[Key words: calcium channels, whole-cell patch clamp, sympathetic ganglion, conotoxin]

ω-Conotoxin fraction GVIA (CgTx), a 27 amino acid highly basic peptide isolated from the venom of the cone snail *Conus geographus* (Olivera et al., 1984), blocks a fraction of the Ca channel current in many vertebrate neurons (Feldman et al., 1987; Kasai et al., 1987; McCleskey et al., 1987; reviewed in Bean, 1989; Hess, 1990). Many studies have shown that CgTx is highly selective for a subset of high-threshold Ca channels (Aosaki and Kasai, 1989; Jones and Marks, 1989; Plummer et al., 1989; Regan et al., 1991; Cox and Dunlap, 1992; Kasai and Neher, 1992; Mintz et al., 1992). Following the demonstration in chick sensory neurons of two types of high-threshold Ca channels, named N-type and L-type, with distinct single-channel characteristics (Nowycky et al., 1986; Fox et al., 1987), Aosaki and Kasai (1989) showed that the smaller-conductance N-type channels were selectively blocked by CgTx. Since then, poorly reversible block by CgTx has been widely adopted as a defining characteristic of N-type Ca channels, and molecular cloning has identified cDNAs in human and rat brain that encode Ca channels blocked by CgTx with the same high potency and poor reversibility as native N-type Ca channels (Williams et al., 1992b; Fujita et al., 1993). Dihydropyridine-sensitive L-type Ca channels have been found to be completely insensitive to high concentrations of CgTx in the vast majority of neurons examined (Aosaki and Kasai, 1989; Jones and Marks, 1989; Plummer et al., 1989; Regan et al., 1991; Cox and Dunlap, 1992; Kasai and Neher, 1992), but occasional individual cells have been encountered where there is partial, reversible block of L-type Ca current (Aosaki and Kasai, 1989; Kasai and Neher, 1992; Mynlieff and Beam, 1992) and a cloned L-type Ca channel was reversibly blocked by high concentrations of CgTx (Williams et al., 1992a), suggesting that the toxin's selectivity may not be absolute.

Despite the utility of CgTx as an N-type Ca channel blocker, many aspects of its action remain unclear. Only limited dose–response data are available. Such basic features as the stoichiometry of its interaction with channels and possible state-dependent binding remain uncharacterized. Electrophysiological studies of CgTx have typically used micromolar concentrations of toxin, while in biochemical studies the K_d for binding is in the picomolar range (Abe et al., 1986; Cruz and Olivera, 1986; Barhanin et al., 1988; Feigenbaum et al., 1988; Wagner et al., 1988). Both binding experiments and electrophysiological studies (McCleskey et al., 1987; Aosaki and Kasai, 1989) have shown that binding or block is weaker in solutions with higher divalent concentrations, but there is little detailed information on such dependence.

We studied these points using frog and rat sympathetic neurons, which have a large fraction of CgTx-sensitive, N-type Ca channel current (Jones and Marks, 1989; Plummer et al., 1989; Jones and Jacobs, 1990; Ikeda, 1991; Regan et al., 1991; Mintz et al., 1992). We found that CgTx block is not voltage dependent and seems independent of the gating state of the channel. The kinetics and potency of CgTx block are consistent with 1:1 binding of toxin to the channel, with estimated K_ds (in 5 mM Ba) of ~30 nM in frog and ~0.1–0.7 nM in rat. With higher Ba concentrations, block is weaker, development of block is slower, and reversal is faster. In experiments with a Ba concentration of 112 mM, saturating concentrations of CgTx and nimodipine leave unblocked a substantial current that has different kinetics and is activated by smaller depolarizations than the CgTx-sensitive N-type current.

Materials and Methods

Preparation of freshly dissociated neurons. Neurons from the sympathetic ganglia of adult bullfrogs (*Rana catesbiana*) were prepared as

Received Nov. 5, 1993; revised Jan. 26, 1994; accepted Feb. 17, 1994.

We thank Drs. Chung-Chin Kuo, Isabelle Mintz, and Kenton Swartz for many helpful discussions and for sharing cells, and Drs. Ann Rittenhouse and Dinah Sah for advice on dissecting superior cervical ganglia. This work was supported by the NIH (HL35034 and NS02253).

Correspondence should be addressed to Bruce P. Bean, Department of Neurobiology, Harvard Medical School, 200 Longwood Avenue, Boston, MA 02115.

previously described (Boland and Bean, 1992) using enzymatic treatment with collagenase and dispase. In a few experiments, neurons were prepared by a different enzymatic treatment of 2 mg/ml collagenase and 3 mg/ml Sigma protease type XXIII for 60–120 min. This treatment gave healthy-looking neurons that readily formed gigaseals and had large Na and Ca channel currents, but the characteristics of CgTx block were different. The onset of CgTx block was similar, but on washing out CgTx, a portion (25–50%) of the current recovered within 10–30 sec, in contrast to the much slower reversal of all the blocked current that was always seen with collagenase/dispase dissociation. Apparently, about half the CgTx-sensitive channels were altered in such a way as to increase greatly the dissociation rate of CgTx (while still being blocked by 3 μM toxin). The results are consistent with a protcolytic effect on the channels, and we did not further study neurons prepared with this dissociation procedure.

Neurons from the superior cervical ganglia of postnatal hooded rats (aged 7–55 d) were prepared by a method based on that of Bernheim et al. (1991). Ganglia were dissected in iced oxygenated Leibovitz's (L-15) medium, connective tissue sheaths were removed, and the ganglia cut in half. Tissue pieces were incubated at 35–37°C in a 0 Ca Tyrode's solution containing (in mM) 150 NaCl, 4 KCl, 2 $MgCl_2$, 10 glucose, 10 HEPES, pH 7.4, plus papain (24 U/ml; Worthington Biochemicals), 2 mM DL-cysteine, and 0.5 m EDTA. After 20 min, the enzyme solution was replaced with a solution containing 1.9 mg/ml collagenase (type I, Sigma) and 16 mg/ml dispase (Boehringer–Mannheim) in 0 Ca Tyrode's. After 45 min at 35–37°C, the tissue pieces were removed from the enzyme solution, placed in oxygenated L-15, and stored at 4°C until use, within 10–12 hr. Tissue pieces were triturated in fresh L-15 medium to yield single cells.

Voltage clamp. Ba currents through voltage-activated Ca channels were recorded using the whole-cell configuration of the patch-clamp technique (Hamill et al., 1981). Patch pipettes were made from borosilicate glass tubing (Boralex, Dynalab, Rochester, NY) or R-6 soda-lime glass (Garner Glass Co.), coated with Sylgard (Dow Corning Corp., Midland, MI), and fire polished.

For whole-cell recordings, pipettes had resistances of 1–4 MΩ when filled with internal solution. Currents recorded with a LIST EPC-7 (Medical Systems, Greenvale, NY) or Dagan 3900A (Dagan Corp, Minneapolis, MN) patch-clamp amplifier were filtered with a corner frequency of 1–10 kHz (4-pole Bessel filter), digitized (10–25 kHz), and stored on a computer. All records were corrected for leak and capacitive currents by subtraction of scaled currents elicited by small hyperpolarizing or depolarizing pulses (−10 to +20 mV from the holding potential, usually −80 mV), which were usually smoothed by fitting points after the first 200 μsec or so by the sum of two exponentials plus a constant. In whole-cell recordings, series resistances ranged from 0.3 to 2.0 MΩ after compensation (typically 80–95%). Only data from cells with series resistances and currents small enough to give a voltage error of less than 5 mV were analyzed.

Experimental data were fitted to equations by nonlinear least squares regression using ORIGIN (MicroCal, Inc., Northampton, MA) or SIGMAPLOT (Jandel Scientific). All statistics are given as mean ± SEM.

Fluctuation analysis was done by the method of Sigworth (1980). Ensembles of currents were generated by a series of identical voltage pulses delivered every 2 sec. Currents were filtered at 3 kHz. The variance was calculated between successive sweeps and then averaged over all the pairs. Single-channel current was estimated by plotting the variance as a function of the mean current and fitting the data by variance $= i \cdot I - I^2/N$.

All experiments were done at room temperature (21–25°C).

Solutions. The standard internal solution consisted of (in mM) 108 CsCl, 9 HEPES, 9 EGTA, 4.5 $MgCl_2$, and an ATP-regenerating solution (Forscher and Oxford, 1985), pH 7.4 with CsOH. The ATP-regenerating solution consisted of (in mM) 14 creatine phosphate (Tris salt; Sigma), 4 Mg-ATP (Sigma), and 0.3 GTP (Tris salt; Boehringer–Mannheim or Sigma), pH 7.4 with Tris base. In some experiments, internal CsCl was replaced by Cs-glutamate with no effect on CgTx block. In experiments with Cs-glutamate, 10 mV was subtracted from the nominal membrane potential to correct for the junction potential between the pipette solution and the bath solution in which the pipette was zeroed prior to contacting a cell. The pipette was sealed to the cell in a modified Tyrode's solution consisting of (in mM) 4 $BaCl_2$, 2 $CaCl_2$, 2 $MgCl_2$, 150 NaCl, 4 KCl, 10 glucose, and 10 HEPES, pH 7.4. Immediately after establishing the whole-cell configuration, cells were lifted from the bottom of the dish, and external solutions were applied by moving the cell or patch in front of a stream of solution applied from one of 10–12 microcapillary tubes (1 μl "microcaps," 64 mm length; Drummond Scientific) glued together side by side and fed by gravity from a reservoir positioned about 0.5 m above. For Ba concentrations of 30 mM or less, $BaCl_2$ was added to 160 mM TEA-Cl, 10 mM HEPES, pH adjusted to 7.4 with TEA-OH. In the solution with 55 mM Ba, the TEA-Cl concentration was reduced to 80 mM. The highest Ba concentration was 112 mM, prepared with 110 mM $BaCl_2$ and 10 mM HEPES, adjusted to pH 7.4 using ~2.5 mM $Ba(OH)_2$. All external solutions contained 1 mg/ml cytochrome C to minimize loss of peptide by binding to glass and plastic. Some solutions (noted in figure legends) contained TTX to block Na channel currents (which were small, very rapid outward currents carried by Cs, since Ba is impermeant in Na channels). In early experiments on frog cells, we added 0.1 mM EGTA to external solutions in order to minimize contamination by trace inorganic blockers (perhaps lead) suspected to be present in some solutions. However, we later found that EGTA slightly slowed the rate of block by 3 μM CgTx, without having any effect on the rate of recovery from block. EGTA was therefore omitted in later experiments, including all of those on the kinetics and concentration dependence of toxin block. The presence of EGTA in some experiments is noted in the figure legends.

Stock solutions of nimodipine (the generous gift of Dr. Alexander Scriabine, Miles Laboratories, West Haven, CT) were prepared in polyethylene glycol and stored in the dark at −20°C. Working solutions of dihydropyridines were prepared immediately prior to use by dilution of the stock solution with the external recording solution (final PEG concentrations were ≤0.2%). ω-Conotoxin (fraction GVIA) was purchased from Peninsula Peptides (Belmont, CA).

Results

Reversibility of ω-conotoxin block

Figure 1 shows experiments in frog (*A*) and rat (*B*) sympathetic neurons in which 3 μM CgTX inhibited the Ca channel current carried by 5 mM Ba. In these and all other experiments, both the control and test external solutions contained at least 3 μM nimodipine to inhibit L-type Ca channels. Nimodipine typically inhibited only a small fraction (5–10%) of current in both frog and rat sympathetic neurons, consistent with previous studies with dihydropyridines (Hirning et al., 1988; Jones and Marks, 1989; Plummer et al., 1989; Regan et al., 1991; Mintz et al., 1992). CgTx (3 μM) blocked all or almost all of the remaining current in both frog and rat neurons. The development of block was strikingly faster in rat (time constant ~ 2 sec) compared to frog neurons (time constant ~ 30 sec). There was also a difference in reversibility. In frog neurons, block slowly reversed after toxin was removed. In cells with particularly stable currents, nearly complete recovery was seen after an hour or so (e.g., Fig. 1*A*); with 5 mM Ba as charge carrier, the average time constant of recovery was 57 ± 7 min ($n = 12$). In contrast, recovery was much slower and less complete in rat neurons, even with wash periods up to 70 min (e.g., Fig. 1*B*). The comparison is complicated by the rundown of calcium channel current that occurs in the absence of toxin, but extrapolating the expected control current in rat neurons showed that substantial reversal would have been seen had it been as fast as in frog. The reversal of block must be at least several times slower in rat neurons than in frog neurons.

In most experiments, the development of block was assayed by depolarizations delivered every 5 sec. However, the depolarizing pulses were not necessary for the development of block. In several experiments with both frog and rat neurons, depolarizations were halted while toxin was applied, and current was completely blocked during the first test pulse given after the application. During washout of toxin from frog neurons, recovery was not altered if depolarizations were delivered at a higher or lower frequency. Block of P-type Ca channels by the spider

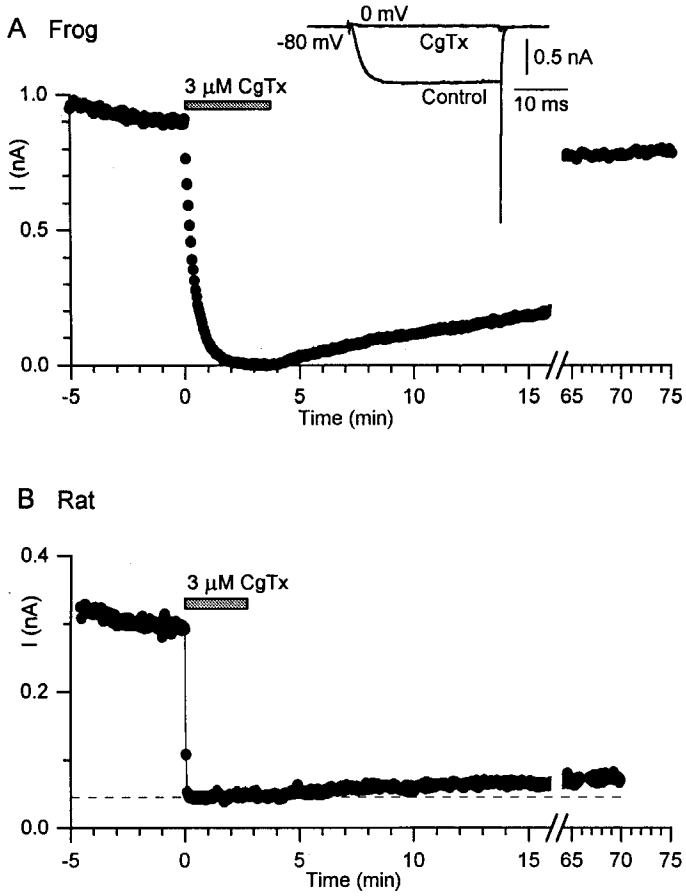

Figure 1. Block by 3 μM CgTx with 5 mM Ba as charge carrier. *A*, Time course of block and recovery from block in a frog sympathetic neuron. Current was evoked every 3 sec by 30 msec voltage steps from a holding potential of −80 mV to a test potential of 0 mV. Current was measured at the end of the test pulse after correcting for leak current (calculated from a step from −80 mV to −70 mV). The block of current could be well fitted with a time constant of 26 sec and the reversal with a time constant of 52 min (not shown). *Inset*, Leak-corrected currents in control and after exposure to CgTx for 3 min. Cell BC42D. *B*, Time course for CgTx block in a rat sympathetic neuron. Current was evoked by 30 msec voltage steps from −80 mV to 0 mV, delivered every 3 sec. Cell BC42E. External solution for both parts: 5 mM $BaCl_2$, 160 mM TEA-Cl, 10 mM HEPES, 3 μM nimodipine, pH 7.4 with TEA-OH.

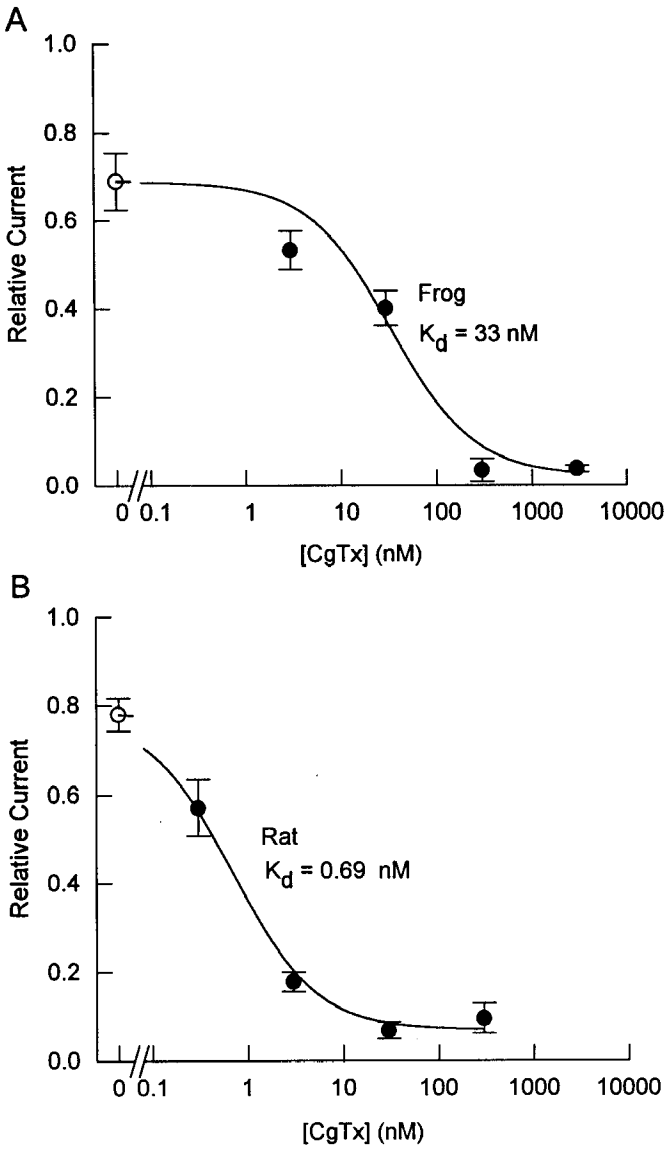

Figure 2. Dose dependence of CgTx block in frog (*A*) and rat (*B*) sympathetic neurons. Data points are the mean (±SEM) fraction of initial current left unblocked after 15 min. The *open symbol* in each plot represents the current remaining after 15 min of rundown in control solution (0.70 ± 0.07 for eight control frog neurons, 0.78 ± 0.04 for six control rat neurons). Determinations for 0.3 nM to 3 μM CgTx were made in three to nine neurons each. *Solid lines* are the best least-square fits to the equation $(y_o - y_t)/(1 + [CgTx]/K_d) + y_t$, where y_o is the fraction of current remaining after 15 min in toxin-free solution, y_t is the fraction of current after block by saturating concentrations of toxin, and K_d is the concentration producing half-maximal block of the toxin-sensitive current. Frog neurons: K_d = 33 nM, y_o = 0.70, y_t = 0.01; rat neurons: K_d = 0.69 nM, y_o = 0.78, y_t = 0.05. External solution: 5 mM $BaCl_2$, 160 mM TEA-Cl, 10 mM HEPES, 3 μM nimodipine, pH adjusted to 7.4 with TEA-OH (all experiments without EGTA in the external solution). Currents were elicited by 30 msec steps from −80 mV to the potential giving maximal current (−10 or 0 mV). Depolarizations were delivered at rates varying from every 10 sec (for toxin-free solutions and low concentrations of toxins) to every second (for higher concentrations).

toxin ω-Aga-IVA can be quickly reversed by a series of large depolarizations (Mintz et al., 1992) but such trains (e.g., ten 50 msec steps to +120 mV delivered at 1 Hz) did not affect N-type channels blocked by CgTx.

Dose dependence of ω-conotoxin block

Figure 2 shows concentration–response relationships for CgTx block in frog (*A*) or rat (*B*) neurons using 5 mM Ba as charge carrier. At the lower concentrations of CgTx (<300 nM in frog and <30 nM in rat), it was impossible to measure true steady-state block because the development of block was so slow that it could not be clearly distinguished from the rundown of current seen in the absence of toxin. We therefore measured block "isochronally" as the amount of block after 15 min. The open symbols at zero toxin concentration represent 15 min applications of toxin-free solution, showing the reduction due to rundown. The data were fitted by curves assuming 1:1 binding and saturating block of 99% for frog cells and 95% for rat cells. From the fits, half-maximal block was obtained with about 30 nM toxin in frog and about 0.7 nM in rat.

Stoichiometry of ω-conotoxin block

What is the stoichiometry of CgTx block of channels? The dose–response relationships in Figure 2 cannot answer this question

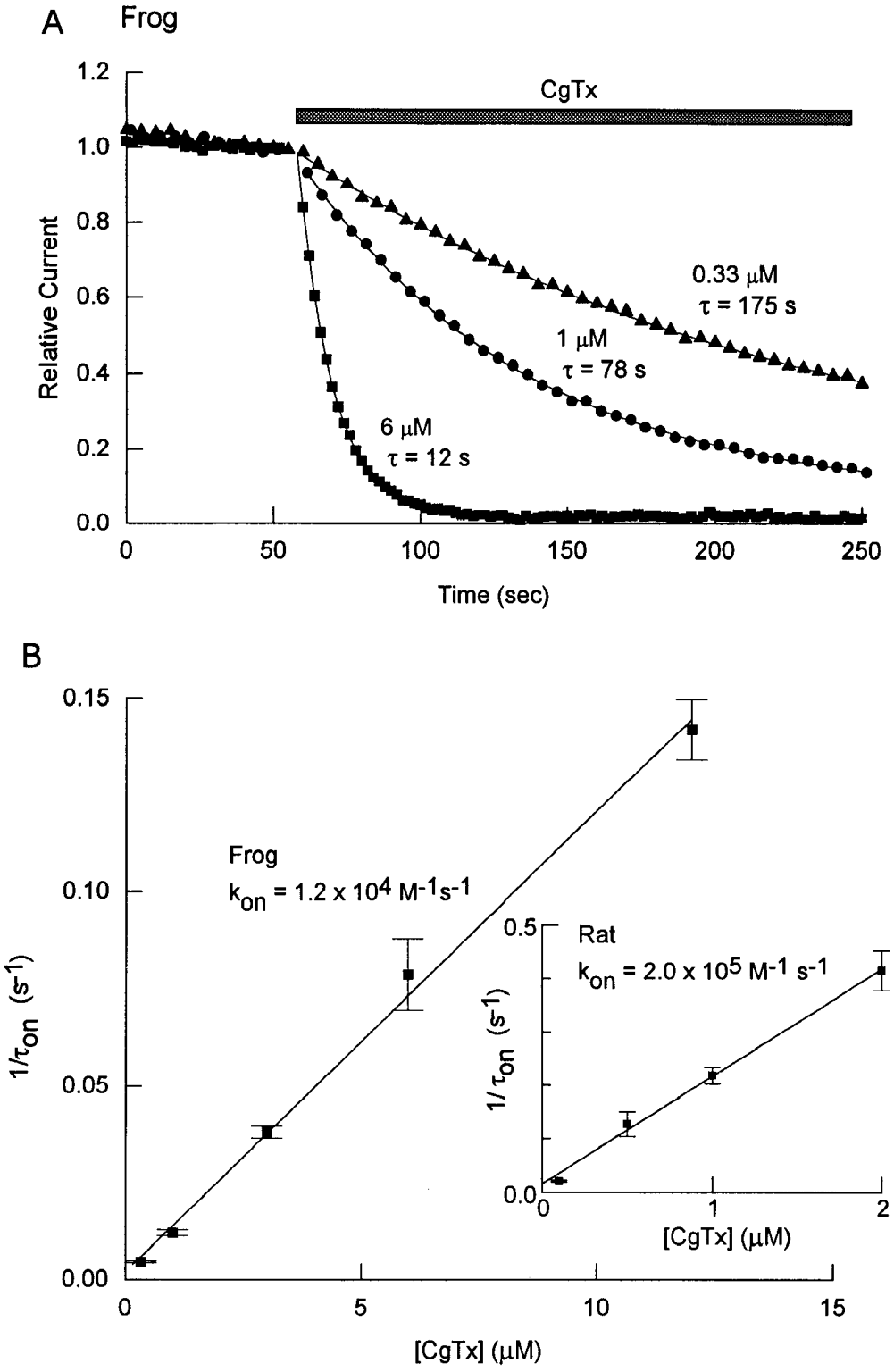

Figure 3. Dose dependence of CgTx blocking rate. *A*, Time course of block in three different frog neurons exposed to 0.33, 1, or 6 μM CgTx. Currents were normalized to the current just before toxin application. *Solid lines* are fits of single exponentials decaying to zero. Current was elicited by 30 msec depolarizations from −80 mV to −10 mV, delivered every 5 sec. *B*, Reciprocal of the blocking time constant versus [CgTx] for frog neurons. Symbols are mean ± SEM for experiments in three cells at each concentration using the protocol shown in *A*. Cells were taken from the same animal to minimize variability. The *solid line* is the best fit (by least-squares) to $1/\tau_{on} = k_{on}$*[CgTx] + k_{off}, the relation expected from mass action for 1:1 binding, with k_{on} = 1.2 × 10^4 $M^{-1}sec^{-1}$ and k_{off} = 2 × 10^{-3} sec^{-1}. k_{off}, which has little effect on the fit, was set based on the reversal data in Figure 10*B*, and k_{on} was varied for the best fit. *Inset*, Reciprocal of blocking time constant in rat neurons. Experiments were done with two batches of rat neurons, prepared from 7- and 8-d-old rats, with three to five cells for each CgTx concentration. Currents were elicited by 30 msec steps from −80 mV to 0 or +10 mV, delivered every 0.5–2 sec. *Solid line* is k_{on}*[CgTx] + k_{off}, with k_{on} = 2.0 × 10^5 $M^{-1}sec^{-1}$ and k_{off} = 0.016 sec^{-1} (the fit was little sensitive to k_{off}, which is certainly too high. With k_{off} set to 0, the best fit for k_{on} was 2.1 × 10^5 $M^{-1}sec^{-1}$). For both frog and rat experiments, the external solution was 5 mM $BaCl_2$, 160 mM TEA-Cl, 10 mM HEPES, 3 μM nimodipine, pH 7.4 with TEA-OH (no EGTA in external solution).

because equilibrium was not reached at low concentrations. We turned instead to measurements of the rate of block as a function of CgTx concentration, using toxin concentrations high enough that block was complete. The time course of block in frog neurons could be fitted well with a single exponential (Fig. 3*A*). For concentrations from 0.33 to 12 μM, block was complete, although only the first 200 sec are shown in Figure 3*A*. The reciprocal of the blocking time constant ($1/\tau_{on}$) is a linear function of CgTx concentration (Fig. 3*B*), suggesting that block results from 1:1 binding of toxin molecules to channel molecules. The slope corresponds to a binding rate constant of 1.2 × 10^4 $M^{-1}sec^{-1}$ for frog neurons. In rat neurons, the rate of block also increased linearly from 0.1 μM to 2 μM (inset, Fig. 3*B*) but the corresponding rate constant is about 20 times higher.

All-or-none block

Several types of experiments showed that if CgTx was applied for a short period so that block was only partial, the properties

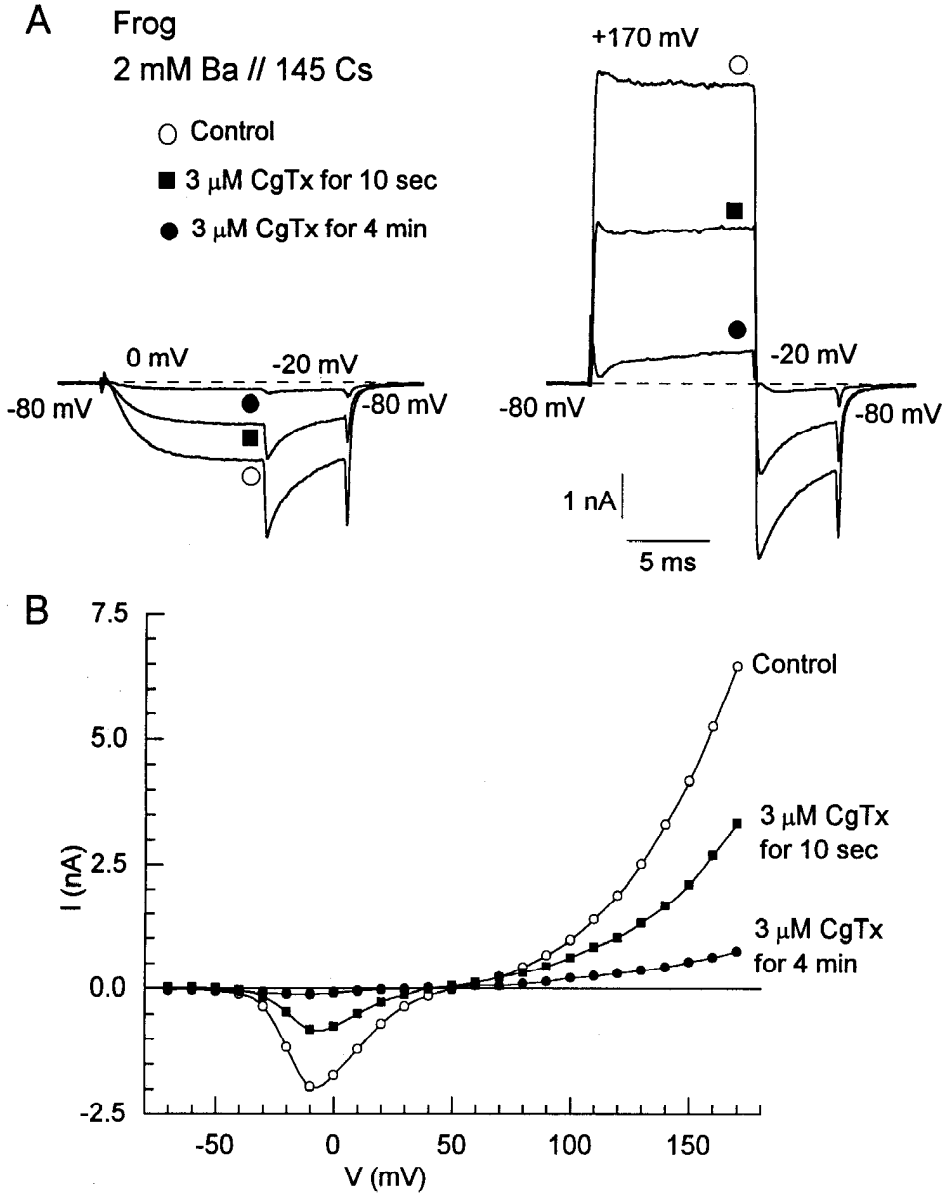

Figure 4. Partial and complete CgTx block at different test potentials in a frog neuron. Currents were elicited by 10 msec steps from −80 mV to test potentials from −70 to +170 mV. *A*, Leak-corrected currents at 0 mV (left) and +170 mV (right) in control, after application of 3 μM CgTx for 10 sec (producing about half maximal block, after which the cell was returned to control solution while the currents at different test potentials were recorded), and after application of 3 μM CgTx for 4 min, producing maximal block. *B*, Current–voltage relationship for test pulse current recorded as in *A*. External solution: 2 mM $BaCl_2$, 160 mM TEA-Cl, 10 mM HEPES, 3 μM nimodipine, 3 μM TTX, pH 7.4 with TEA-OH (no EGTA in external solution). Cell BC34D.

of the unblocked channels were identical to those in control. Figure 4 shows the voltage dependence of Ca channel currents in control, after 3 μM toxin applied for 10 sec blocked about 50% of the current, and after further exposure to 3 μM toxin for several minutes produced maximal block. With partial block by the short application of CgTx, currents were blocked to about 50% at all voltages, regardless of whether current was inward, carried by Ba ions, or outward, carried by Cs ions. With saturating block, Ca channel current was blocked nearly completely at all potentials. In this cell, a small fraction of inward current (~6% at −10 mV) remained unblocked, but in most other cells there was no such current remaining. The small outward current at very positive potentials that remained in this experiment after saturating CgTx block could be partly through the small fraction of unblocked Ca channels and partly through other channels (e.g., Cs flowing through potassium channels). Similarly, when partial block of the whole-cell current was produced by short applications of CgTx, both the voltage dependence of inactivation (Fig. 5) and the single-channel current estimated from fluctuation analysis (Fig. 6) were unaltered from control. The results are consistent with all-or-none block of individual channels, so that when a channel is blocked it is incapable of passing any current, either inward or outward. The results further suggest that once established, block is not readily reversed or enhanced by depolarization; neither short (10 msec) depolarizations up to +170 mV (Fig. 4) nor longer (2 sec) depolarizations up to −10 mV (Fig. 5) affect the amount of block.

Effects of divalent concentration on blocking rate

The development of CgTx block was slower in higher Ba concentrations in both frog and rat neurons. Figure 7*A* compares the rate of block by 3 μM CgTx in two different frog neurons, one with current carried by 5 mM Ba, where block developed with a time constant of 29 sec, and one studied with current carried by 30 mm Ba, where block developed with a time constant of 354 sec (block was eventually complete in the 30 mM Ba solution, although only the first 150 sec are shown). In rat neurons, block was also slower when higher Ba solutions were used. Figure 7*B* shows examples, with 3 μM CgTx blocking with a time constant of 2.4 sec in 5 Ba and 7.6 sec in 30 mM Ba.

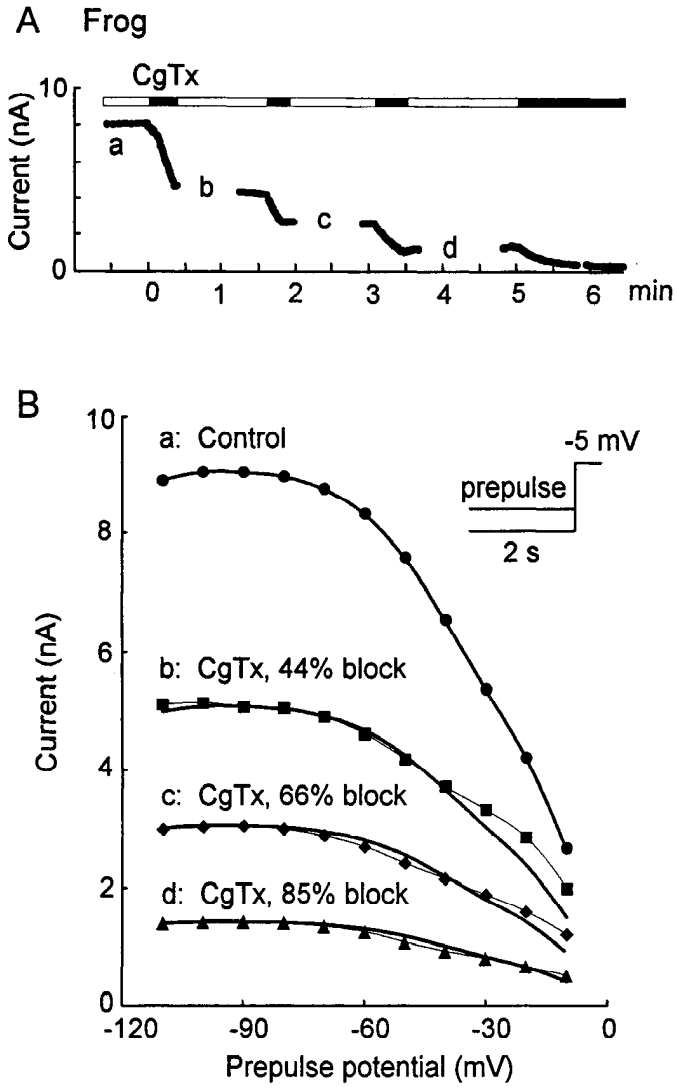

Figure 5. Effect of inactivation on CgTx block in a frog neuron. *A*, Experimental protocol showing the brief applications of 3 μM CgTx (*solid bars*) to produce increasing amounts of partial block in a frog neuron. During the partial block by toxin, inactivation curves were obtained by assaying the test current at −5 mV following a series of 2 sec prepulses from −110 mV to −10 mV. *B*, Ba current amplitudes were determined at the points indicated on the time course by control (*a*), after 44% block by CgTx (*b*), after 66% block by CgTx (*c*), and after 85% block by CgTx (*d*). *Thin lines* connect the data points; *thick lines* are scaled versions of the control curve with scaling factors of 0.56 (*b*), 0.34 (*c*), 0.15 (*d*). External solution: 5 mM $BaCl_2$, 160 mM TEA-Cl, 10 mM HEPES, 0.1 mM EGTA, 3 μM nimodipine, 1.5 μM TTX, pH 7.4 with TEA-OH.

In frog neurons, there was a roughly linear relationship between the time constant of block and the concentration of Ba. For example, the time constant for block by 3 μM CgTx was 44 ± 3 sec at 5 mM Ba (n = 25) and 493 ± 51 sec at 55 mM Ba (n = 4). A simple possibility is that CgTx competes with Ba for a binding site that either can occupy. In this case, the rate of block by CgTx would be proportional to the fraction of sites not occupied by Ba. For simple 1:1 binding of Ba to the binding site, the fraction of sites not occupied by Ba would vary linearly with Ba at concentrations well above the K_d for Ba binding. In Figure 7*C*, the rate constant for block by 3 μM CgTx (calculated as the reciprocal of the time constant divided by 3 μM) is plotted versus Ba concentration on a log–log scale. The data are reasonably well fitted by a line of slope −1, as would result if all the Ba concentrations (from 0.5 to 55 mM) are well above the K_d for Ba binding to the hypothetical binding site. The solid lines in the figure show the predicted relationship between the rate constant for CgTx block and Ba concentration assuming binding sites with different K_ds for Ba binding. The data are consistent with K_ds below about 100 μM.

Effects of ionic strength on CgTx kinetics

In the experiments varying Ba shown in Figure 7, the effects could be due either to a specific effect of Ba or a consequence of the higher ionic strength of the solutions with higher $BaCl_2$. An effect of ionic strength on blocking kinetics would be expected. Many ion channels behave as if there is a negative surface potential on or near the channel (reviewed by Hille, 1992). Such a surface potential would serve to concentrate a positively charged molecule like CgTx (net charge of +5 predicted at neutral pH). Solutions of higher ionic strength would reduce the surface potential produced by negative charges on or near the channel and thus produce a lower local concentration of CgTx and slower block.

To test the effects of ionic strength independent of specific effects of Ba, we varied the concentrations of monovalent ions while studying CgTx block in solutions containing 2 mM Ba to carry charge. CgTx block was dramatically faster in a low-ionic-strength solution of 2 mM $BaCl_2$ in 300 mM sucrose (with 10 mM HEPES and ~5 mM TEA-OH) than with a "standard" solution with 160 mM TEA-Cl in place of the sucrose (Fig. 8*A*). CgTx (0.5 μM) blocked with an average time constant of 9 ± 1 sec (n = 6) in the sucrose solution and with a time constant of 71 ± 3 sec (n = 5) in the standard TEA-Cl solution. Similarly, further increasing the ionic strength by adding 100 mM CsCl to the standard solution resulted in slower block (Fig. 8*B*). CsCl was selected to increase the ionic strength since it was found to be nearly "inert" for permeation through L-type Ca channels (Kuo and Hess, 1992); consistent with this, addition of 100 CsCl had almost no effect on current in the standard TEA-Cl solution in the same cell. CgTx (3 M) blocked with an average time constant of 12 ± 1 sec (n = 5) in the standard TEA-Cl solution and with a time constant of 22 ± 3 sec (n = 8) in the same solution with 100 mM CsCl added.

Figure 8*C* shows the collected results of experiments varying TEA-Cl and CsCl. When the time constant of block was converted to a first-order rate constant for blocking, this was the same for block by 0.5 μM CgTx and 3 μM CgTx in the standard solution, consistent with 1:1 binding of toxin to receptor. Compared to the standard TEA-Cl solution (ionic strength, 171 mM), block was ~10 times faster in the sucrose-containing solution (ionic strength, 11 mM) and ~40% slower in the CsCl-containing solution (ionic strength, 271 mM). Figure 8*D* shows that these results can be fitted well by simple Gouy-Chapman theory assuming that there is a negative surface charge of −0.004 e/Å^2 near the channel and that the toxin molecule behaves with an equivalent valence of +2. These values were determined by trial and error calculations with different surface charges and effective valences.

Using these parameters for surface charge and effective valence of CgTx, Figure 8*D* shows how the rate of CgTx is predicted to vary in solutions with different amounts of $BaCl_2$ (in solutions of 160 mM TEA-Cl, as for the experimental determinations in Fig. 7) if the only effect is to screen surface charge. The predicted

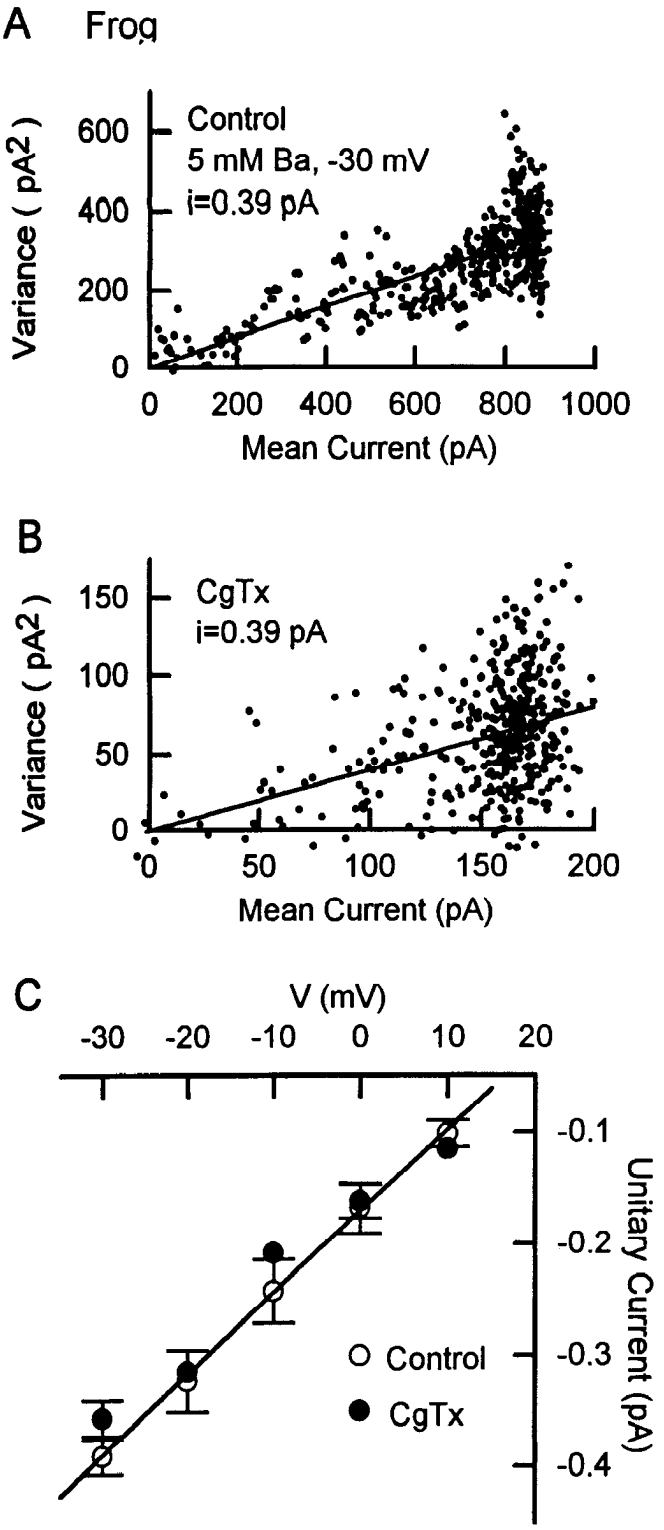

Figure 6. Noise analysis of partial CgTx block in frog neurons. Currents were elicited by voltage pulses from −80 mV to −30 mV, applied every 2 sec, and sampled at 20 μsec after filtering at 3 kHz (4-pole Bessel). After recording a series of 42 control pulses, CgTx (3 μM) was applied for about 15 sec until current was blocked by about 80%, and a series of 38 pulses was then recorded. The variance at each time point was calculated for each pair of successive currents and averaged over the pairs for each series. Background (non-Ca channel) variance was calculated for the points at −80 mV before the depolarization, and this value was subtracted from the variance during the depolarization. *A*, Variance versus mean current for the control series of pulses. Background variance of 65 pA² was subtracted. Data were fitted by least-squares to the relation expected for noise from homogeneous, independent channels: variance = $i \cdot I - I^2/N$, where i is the unitary current, I is the mean current, and N is the number of functional channels. The line is drawn for i = 0.39 pA, N = 57,280. Since the fitted parabola is not far from a straight line, the fit is not very sensitive to the value of N, which is therefore not well determined. The first 160 μsec of the test current was omitted due to imperfectly corrected capacitative transients. *B*, The same analysis for currents after partial CgTx block. Background variance of 64 pA² was subtracted. The line is the best least-squares fit, with i = 0.39, N = 12,327. The fit is close to a straight line and is not sensitive to the value of N. Cell LD16C. *C*, Unitary current estimated from noise analysis versus test potential for control currents (*open circles*) and currents after partial (70–85%) CgTx block (*solid circles*). Data points are the means ± SEM for three to five cells, except for CgTx data at −20, −10, and +10 mV, which are the average from two cells. Unitary current for an individual cell was obtained as the average of two or three determinations in the cell. The line (slope = 7.3 pS) was fitted by linear regression to the control data from −30 to 0 mV. External solution: 5 mM $BaCl_2$, 160 mM TEA-Cl, 10 mM HEPES, 0.1 mM EGTA, 10 μM nimodipine, 3 μM TTX, pH 7.4 with TEA-OH.

changes in the rate of block are far less than seen experimentally, especially at low Ba concentrations. The comparison suggests that the effects of Ba on blocking kinetics are larger than can be explained by simple surface charge screening.

CgTx block in the presence of Cd

Ca channels can be blocked by inorganic ions such as Cd, which probably bind at the same sites as are occupied by Ca and Ba during the permeation process. If CgTx binding also involves one of these sites, CgTx binding might be affected by the presence of Cd. We therefore tested for possible effects of Cd on the rate of CgTx binding. Such an experiment is shown in Figure 9*A*. Application of 1 μM $CdCl_2$ in an external solution containing 5 mM Ba inhibited about 75% of the current. Subsequent addition of 3 μM CgTx resulted in complete block of the remaining current with a time constant of 30 sec, similar to the rate of block in experiments without Cd present. In collected experiments done under the same conditions, 3 μM CgTx blocked with a time constant of 23 ± 3 sec in the presence of 1 μM Cd (n = 7) and a time constant of 21 ± 4 sec in the absence of Cd. The binding rate of CgTx is apparently not affected by partial block by Cd.

Effects of divalent concentration on recovery rate

In addition to changing blocking kinetics, the concentration of Ba affected the rate of recovery from CgTx block (Fig. 10), but not nearly as dramatically. In frog neurons, recovery from block was about threefold faster in 112 mM external Ba (mean recovery time constant 21 ± 2 min, n = 9) than in 5 mM Ba (57 ± 7 min, n = 12). In the simplest mechanisms whereby CgTx would occupy a binding site that could also be occupied by Ba, there would be no acceleration of CgTx unbinding by Ba ions. But since the permeation pathway of the Ca channel can be occupied by multiple Ba ions (Hess and Tsien, 1985; Kuo and Hess, 1993a–c), it is possible that CgTx can bind to channels that are occupied by one or more Ba ions. If so, CgTx might compete with Ba at a site to which Ba can bind very tightly (consistent with the data in Fig. 7) but Ba might be present in CgTx-blocked channels at another site with lower affinity for Ba, which could be occupied by Ba at high millimolar concentrations of Ba but not lower concentrations. Ba, at this second site, might speed CgTx unbinding by electrostatic repulsion. If such a second Ba binding site is internal to the higher-affinity site for which Ba and CgTx compete, it might be inaccessible when the channel

←

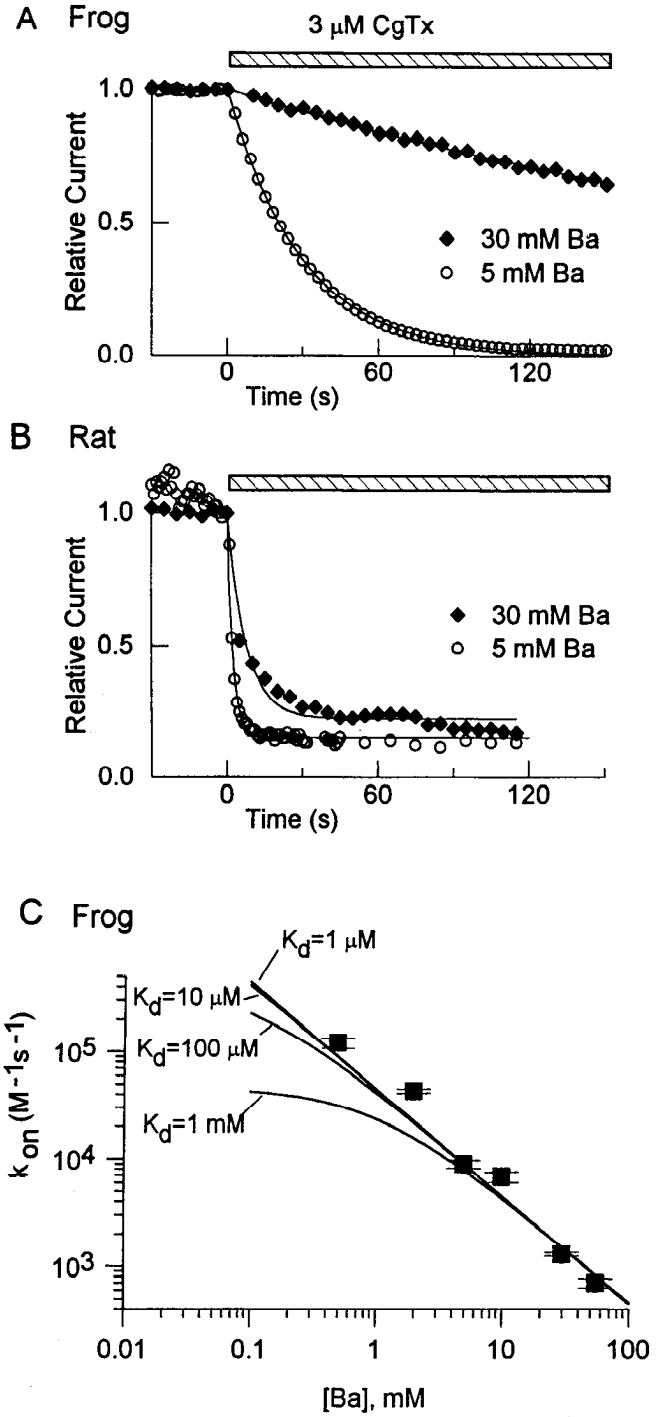

Figure 7. Effect of Ba concentration on CgTx blocking rate. *A*, The time course of 3 μM CgTx block in 30 mM Ba (*solid triangles*) or 5 mM Ba (*open circles*), in two frog neurons. Currents are normalized to the size at the time of toxin application. *Solid lines* are single exponentials decaying to zero, with time constants of 354 sec for 30 mM Ba and 29 sec for 5 mM Ba. Cells JB12C and JB22A. *B*, Block by 3 μM CgTx in 30 mM Ba (*solid triangles*) or 5 mM Ba (*open circles*), in two rat neurons. Solid line fitted to 30 mM Ba data is a single exponential of time constant 7.6 sec decaying to a steady-state value of 0.22. Solid line fitted to 5 mM Ba data is a time constant of 2.4 sec decaying to a steady-state of 0.15. Cells JB73C and JB91A. *C*, Rate constant of block versus Ba concentration in frog neurons. Data points are the inverse of the time constant of block (mean ± SEM, n = 4–35). Currents were evoked by voltage steps to voltages near the peak of the current–voltage relationship; these ranged from −20 mV (in 0.5 mM Ba) to +20 mV (in 55 mM Ba). The interpulse interval was 5 sec (for 0.5–10 mM Ba) or 8 sec (30–55 mM Ba). The *solid lines* are drawn according to $k_0/(1 + [Ba]/K_d)$, the relation expected if CgTx competes with Ba for a binding site, where k_0 is the hypothetical rate of block of CgTx with no Ba and K_d is the dissociation constant for Ba binding to the site. Lines are drawn for K_d = 1 mM (with $k_0 = 4.7 \times 10^4$ $M^{-1}sec^{-1}$), K_d = 100 μM (with $k_0 = 4.7 \times 10^5$ $M^{-1}sec^{-1}$), K_d = 10 μM (with $k_0 = 4.7 \times 10^6$ $M^{-1}sec^{-1}$), and K_d = 1 μM (with $k_0 = 4.7 \times 10^7$ $M^{-1}sec^{-1}$). External solutions: 0.5–55 mM $BaCl_2$, 160 mM TEA-Cl (80 mM TEA-Cl with 55 mM $BaCl_2$), 0.1 mM EGTA (frog data only), 10 mM HEPES, pH adjusted to 7.4 with TEA-OH.

is blocked by CgTx. In this case, a channel blocked by CgTx applied in 5 mM Ba might recover with a rate typical of that with 5 mM Ba if the external solution is switched to 112 mM Ba after complete block has been produced in 5 mM Ba. Such an experiment is shown in Figure 10*A*. Contrary to the expectations of this simple model, recovery from block was accelerated immediately on changing from 5 mM Ba (recovery time constant, 88 min) to 112 mM Ba (time constant, 17 min). Evidently the CgTx binding is somehow destabilized by external Ba ions, not just by Ba ions trapped inside the channel.

Since CgTx binding is slower in higher Ba, and CgTx unbinding is faster, the dissociation constant of CgTx binding must be considerably higher in 112 Ba compared to 5 mM Ba. In frog neurons studied with 112 Ba, the binding rate constant is 7×10^2 $M^{-1}sec^{-1}$ (Fig. 7*C*) and the unbinding rate constant is $8\ 10^{-4}$ sec^{-1} (Fig. 10*B*), giving a calculated K_d of 1.1 μM. This can be compared to the K_d of 33 nM measured in 5 mM Ba.

For the rat neuron studied with 112 Ba in Figure 10*C*, the onset of block could be fitted by a time constant of 13 sec, and the recovery was fitted with a time constant of 20 min (fit assuming partial recovery to 0.7 nA), or a time constant of 40 min (fit assuming eventual complete recovery). These on and off rate constants correspond to a K_d of 0.2–0.4 μM in 112 mM Ba. This implies 500–1000-fold weaker binding of CgTx in 112 Ba compared to 5 Ba.

Current remaining unblocked by CgTx and nimodipine

In many frog neurons, application of saturating concentrations of CgTx in the presence of 3 μM nimodipine blocked all of the inward current elicited by depolarizations (e.g., Fig. 1*A*). In some frog neurons, though, clear inward current remained. A small component of current resistant to both dihydropyridines and CgTx was previously reported by Jones and Jacobs (1990).

As will be discussed, the current resistant to both blockers was most prominent in solutions containing high Ba concentrations. However, in some cells, such current could be clearly detected in solutions containing 2 mM Ba. An example is shown in Figure 11. In this cell, where all solutions contained 10 μM nimodipine, application of 3 μM CgTx greatly reduced both inward and outward currents activated by depolarizations, with the CgTx-sensitive current reversing polarity at about +50 mV. However, a clear depolarization-activated inward current remained with nimodipine and CgTx, producing a peak inward current of ~300 pA at −20 mV (Fig. 11*B*). This represents about 5% of the 6 nA inward current before CgTx. The resistant current had a slightly different voltage dependence, reaching a peak at −20 mV while the CgTx-sensitive current peaked at −10 mV. CgTx had little effect on current activated at −50 mV, where depolarization-activated current first became detectable, and inhibited the current at −40 mV by less than half. Apparently the resistant current activates over a slightly more negative voltage range than the CgTx-sensitive current. This

might be consistent with low-threshold T-type current, but the resistant current did not have the kinetic characteristics of T-type current, which include rapid inactivation and slowly deactivating tail currents. Figure 11*C–E* compares the kinetics of the resistant current at −20 mV with those of the predominant CgTx-sensitive current. Both the CgTx-sensitive current and the resistant current deactivated quickly at −80 mV; while the deactivation time constant for the resistant current (0.46 msec) was significantly slower than that of the CgTx-sensitive current (0.17 msec), both are much faster than the tail time constants of several msec seen for T-type channels in frog sensory neurons under similar conditions (B. P. Bean, unpublished observations). The activation kinetics of the resistant current were also different than those of the CgTx-sensitive current, the resistant current activating with a predominant time constant of 1.1 msec and the CgTx-sensitive current with a time constant of 2.8 msec. The different voltage dependence and kinetics of the resistant current compared to the CgTx-sensitive current suggests that the two are carried by distinct channel types, rather than reflecting incomplete block by CgTx of a single class of channels.

The current resistant to both nimodipine and CgTx was more prominent in experiments using higher Ba concentrations to carry the current. Even in cells where there was little or no resistant current with 2 mM Ba as charge carrier, there was a sizeable fraction of current that remained unblocked when 112 mM Ba was used as charge carrier. An example is shown in Figure 12. In this cell, current–voltage relationships were determined with both 2 mM Ba and 112 mM Ba in solutions containing 10 μM nimodipine. CgTx (30 μM) was then applied in 2 mM Ba and produced rapid and complete block of the current at all potentials (closed circles in Fig. 12*B*). When the solution was switched to 112 mM Ba (also containing 30 CgTx with 10 μM nimodipine), however, there was a current of ~2 nA evident within a few seconds of changing the solution. The current in 112 Ba was not due to unbinding of CgTx from the channels, since current in 2 mM Ba remained completely blocked when the cell was quickly transferred back and forth between the two solutions (Fig. 12*A*).

Figure 12*C* shows the current–voltage relationship for current carried by 112 mM Ba. The resistant current activates over a more negative voltage range than the CgTx-sensitive current, producing significant current at −40 to −10 mV that is almost unaffected by CgTx. Both the resistant current and the CgTx-sensitive current reverse at ~+70 mV, consistent with an equally high selectivity for Ba over Cs. As for the results with 2 mM Ba in Figure 11, the different voltage dependence of resistant current is reminiscent of T-type current, but unlike T-type current, the resistant current has rapidly deactivating tail currents (Fig. 12*C*, inset). The resistant current apparently inactivates somewhat faster than the CgTx-sensitive current, decaying by 20–25% during the 30 msec steps used in this experiment, but T-type channels would show much more prominent inactivation under these conditions.

A similar nimodipine- and CgTx-resistant current was seen in rat sympathetic neurons, where it was also more prominent in conditions with high Ba concentrations. In rat sympathetic neurons, a current remaining in nimodipine and CgTx was almost always evident in solutions with 5 mM Ba as charge carrier, and this resistant current was a larger fraction of the total current in solutions with higher Ba concentrations. Figure 13 shows an example. In this cell, with 112 mM Ba as charge carrier, 30 μM CgTx blocked about 70% of the current in the continuous presence of 3 μM nimodipine. To check if the concentrations of nimodipine or CgTx were saturating, both were then increased. Increasing nimodipine from 3 μM to 10 μM nimodipine had no effect on the remaining current, and increasing CgTx from 30 μM to 100 μM also had no effect on the current (Fig. 13*B*). These were consistent observations. Increasing the CgTx concentration from 30 μM to 100 μM had no further effect in each of three cells, and in collected results, 30 μM CgTx blocked 69 ± 35% ($n = 6$) and 100 μM CgTx blocked 72 ± 3% ($n = 6$) of the current (with 112 mM Ba carrying current in the presence of 3 μM nimodipine). Increasing the nimodipine concentration from 3 to 10 μM (Fig. 13*A*) produced no further block of the current in each of three cells. As in frog neurons, the resistant current in rat neurons did not have the characteristics of T-type current. Depolarizing the holding potential from −80 mV to −40 mV, which would be expected to inactivate T-type current completely under similar conditions, reduced the resistant current by ~35% but did not eliminate it. The resistant current had tail currents at −80 mV that were nearly as rapidly deactivating ($\tau = 0.59$ msec) as those of the CgTx-sensitive current ($\tau = 0.46$ msec). As in frog neurons, the resistant current activated with a predominant time constant that was faster than that of the CgTx-sensitive current (Fig. 13*C*).

As in frog neurons, the current resistant to both nimodipine and CgTx in rat neurons activated over a more negative voltage range than the CgTx-sensitive current (Fig. 14*A*), so that the current elicited by depolarizations in the range of −10 to +10 mV in 112 mM Ba is almost entirely resistant to block by CgTx and nimodipine. In the cell whose results are shown in Figure 14, as for that depicted in Figure 13, the resistant currents have fast tail currents. As in frog neurons, the resistant current shows somewhat faster inactivation kinetics than the CgTx-sensitive current (Fig. 14*B,C*). This is particularly evident for larger depolarizations (Fig. 14*C*), but even for the step to +30 mV shown in Figure 14*C*, the resistant current decays by only about 25% during a 30 msec step, much slower than would be expected for T-type current.

Discussion

Potency, stoichiometry, and reversibility

CgTx blocked the great majority of Ca channel current in both frog and rat sympathetic neurons. In the experiments reported here, we used solutions containing nimodipine to block L-type Ca channels, which have previously been found to make up only 5–10% of the overall high-threshold current in both frog and rat sympathetic neurons. With L-type channels blocked, CgTx blocked an average of ~97% of the remaining current in frog neurons and ~90–95% of the remaining current in rat neurons when studied with 5 mM Ba as charge carrier. These results are consistent with previous results.

There were significant differences in the characteristics of CgTx block between frog and rat sympathetic neurons. Block was more potent, developed faster, and reversed more slowly in rat neurons than in frog neurons. In both frog and rat neurons, toxin molecules seem to block channels with a 1:1 binding reaction, since the rate of block is a linear function of toxin concentration (Fig. 3). Although the time course of reversal of block was very slow in frog neurons, with an average time constant of 58 min, it was even slower in rat neurons, such that in most neurons no reversal was detectable. In frog neurons, the unbinding rate constant is 2.9×10^{-4} sec^{-1}. Together with the binding rate constant of 1.2×10^{4} M^{-1}sec^{-1} and assuming a 1:1

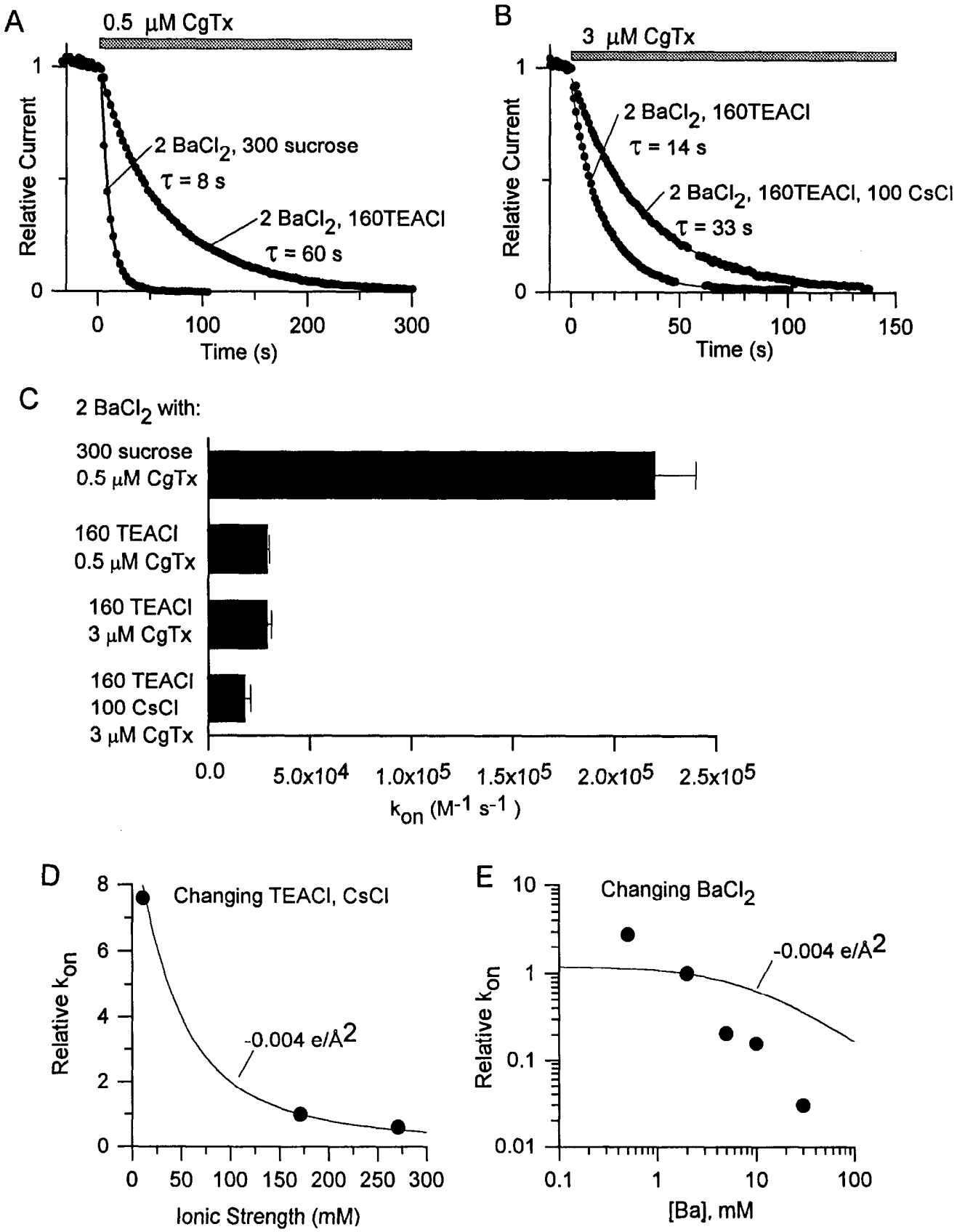

Figure 8. Effect of ionic strength on rate of CgTx block. *A*, The time course of block by 0.5 μM CgTx in low-ionic-strength external solution compared to that in the standard solution. Experiments were done with two frog neurons from the same dissociation. Low-ionic-strength solution consisted of 2 mM $BaCl_2$, 300 mM sucrose, 10 mM HEPES, pH adjusted to 7.4 with ~5 mM TEA-OH. Standard solution consisted of 2 mM $BaCl_2$,

binding reaction (see below), a K_d of 28 nM is predicted in frog neurons. This is similar to the K_d of 33 nM estimated directly from the amount of block by different concentrations (Fig. 2). In rat neurons, the K_d of 0.69 nM from the fitted dose–response curve is certainly an overestimate, since 15 min is not long enough to reach steady-state block at lower toxin concentrations. The off rate in rat neurons is too slow to be measured accurately, but a lower limit can be estimated as $\sim 2 \times 10^{-5}$ sec^{-1}, since there is detectable (more than a few percent) recovery in 15–20 min in some rat cells (e.g., Fig. 1*B*). (An upper limit of $\sim 2 \times 10^{-4}$ can be estimated, since this would give ~10% recovery in 10 min, which could have been seen easily in most cells.) Together with the forward rate constant of $\sim 2.0 \times 10^5$ M^{-1}sec^{-1} from Figure 3, the lower limit estimate of k_{off} would give a lower limit estimate of 0.1 nM for the K_d in rat neurons. Thus, the dose–response data in Figure 2 and the comparison of kinetics suggest that the binding affinity in rat neurons is between 50-fold and 300-fold higher than in frog neurons.

The K_d of 0.1–0.7 nM for N-type channels in rat neurons, determined with a 5 mM $BaCl_2$, 160 mM TEA-Cl solution, can be compared with K_ds of 0.8–60 pM estimated from binding of iodinated CgTx to rat brain membranes (Feigenbaum et al., 1988; Wagner et al., 1988), determined in divalent-free sucrose solutions. It seems likely that the difference in K_ds is mainly accounted for by the different ionic conditions. Interestingly, the difference is mainly in the on rate for toxin binding, since the off rate of $\sim 10^{-5}$ sec^{-1} found in the binding experiments (Feigenbaum et al., 1988; Wagner et al., 1988) is only ~20-fold lower than the upper limit of 2×10^{-4} sec^{-1} that we estimate from electrophysiological experiments. Consistent with this, our experiments show a very strong dependence of on rate with divalent concentration (Fig. 7).

All-or-none block

All of the results are consistent with the idea that toxin molecules bind and unbind slowly and that a channel is completely blocked when toxin is bound. Toxin blocked outward as well as inward current, and block was equal at different test potentials and after 2 sec prepulses to different potentials. Thus, block is not modulated by voltage, at least not on the time scale of milliseconds to seconds. This is consistent with toxin binding equally well to different gating states (resting, open, and inactivated) of the channel and is in striking contrast to block of P-type Ca channels by the spider toxin ω-Aga-IVA, where block can be reversed within hundreds of msec by strongly activating depolarizations (Mintz et al., 1992; I. M. Mintz and B. P. Bean, unpublished results).

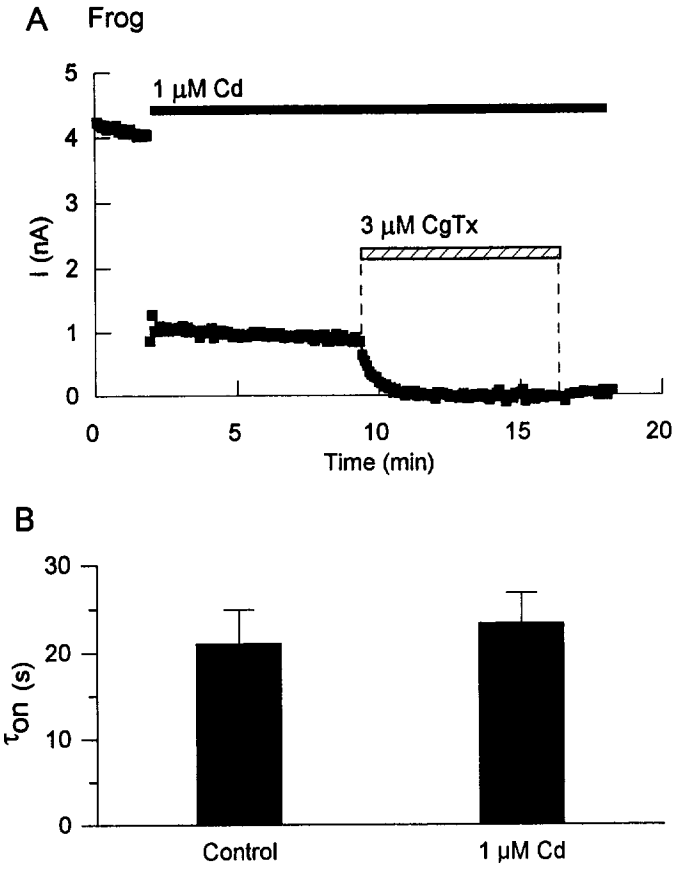

Figure 9. CgTx block in the presence of Cd. *A*, Time course of leak-corrected Ba current in a frog neuron evoked by a test pulse from −80 mV to 0 mV, showing the effect of 1 μM Cd and subsequent addition of 3 μM CgTx in the presence of Cd. The decline of current after addition of CgTx is fitted by a time constant of 30 sec (a solid line that overlaps with the data points). *B*, Time constant (mean ± SEM) for block by 3 μM CgTx in the absence ($n = 4$) or presence ($n = 7$) of 1 μM Cd. External solution: 5 mM $BaCl_2$, 160 mM TEA-Cl, 3 μM nimodipine, 10 mM HEPES, pH 7.4 with TEA-OH (no EGTA in the external solution).

Effect of ionic strength and Ba on binding kinetics

One of the goals of this work was to understand better the dependence of CgTx blocking kinetics on divalent concentra-

←

160 mM TEA-Cl, 10 mM HEPES, pH adjusted to 7.4 with ~5 mM TEA-OH. Currents are normalized to the size at the time of toxin application. *Solid lines* are single exponentials with time constants of 8 sec for the low-ionic-strength solution and 60 sec for the standard solution. Cells BC40K and BC40G. *B*, The time course of block by 3 μM CgTx in standard solution compared to that in a high-ionic-strength solution (2 mM $BaCl_2$, 160 mM TEA-Cl, 100 mM CsCl, 10 mM HEPES, pH adjusted to 7.4 with ~5 mM TEA-OH). *Solid lines* are single exponentials with time constants of 14 sec for the standard solution and 33 sec for the standard solution. Cells BC41F and BC41N. *C*, Collected results for solutions with 2 mM $BaCl_2$ and variable monovalent ions. The first-order blocking rate constant was calculated as $1/(\tau \cdot [\text{CgTx}])$. Values are $2.2 \pm 0.2 \times 10^5$ M^{-1}sec^{-1} for low-ionic-strength solution with 0.5 μM CgTx ($n = 6$), $2.9 \pm 0.1 \times 10^4$ M^{-1}sec^{-1} for standard solution with 0.5 μM CgTx ($n = 5$), $2.9 \pm 0.2 \times 10^4$ M^{-1}sec^{-1} for standard solution with 3 μM CgTx ($n = 5$), and $1.8 \pm 0.1 \times 10^4$ M^{-1}sec^{-1} for high-ionic-strength solution with 3 μM CgTx ($n = 8$). *D*, k_{on} relative to that in standard solution is plotted versus ionic strength. *Smooth line* is calculated from Gouy-Chapman theory assuming a surface charge of −0.004 electron charges/Å^2 and an effective valence of +2 for the CgTx molecule. For each ionic solution, the Grahame equation was solved iteratively to obtain the surface potential, and this potential was used in the Boltzmann equation to calculate the surface concentration of CgTx relative to that in the bulk solution. Relative k_{on} is proportional to the concentrating factor relative to that for standard solution. Values of surface charge and effective valence were systematically varied (over ranges of 0.001 to −0.03 e/Å^2 and +1 to +6 valence, respectively) to find the prediction closest to the data. *E:Line* is predictions for k_{on} relative to that in the standard solution, calculated for a surface charge of −0.004 e/Å^2 and effective valence of +2, when $BaCl_2$ is varied in a solution of 160 mM TEA-Cl, 10 mM HEPES, pH 7.4 with 5 mM TEA-OH. *Points*, Experimental data replotted from Figure 7.

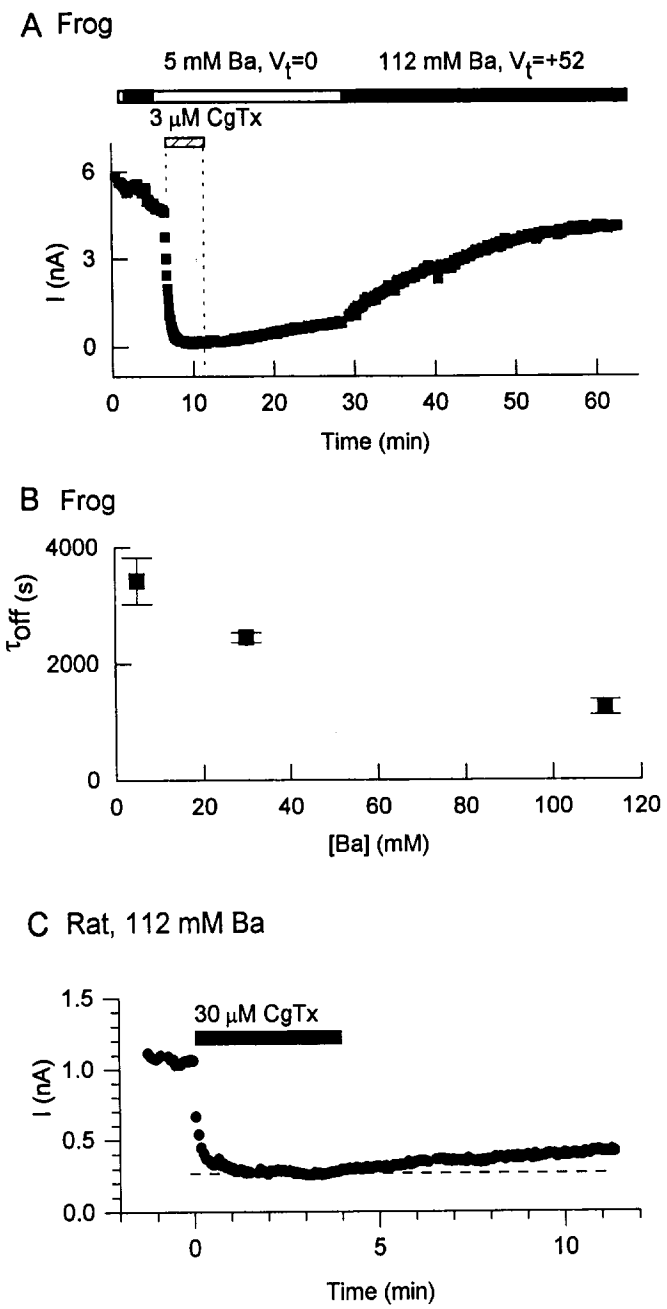

Figure 10. Effect of Ba concentration on recovery from CgTx block. *A*, Acceleration of recovery from CgTx block in a single frog neuron in which the Ba concentration was raised from 5 mM to 112 mM during the recovery phase. The test potentials used were 0 mV in 5 mM Ba and +52 mV in 112 mM Ba, chosen to give nearly equal current amplitudes in the control solutions. The recovery in 5 mM Ba is fitted with an exponential of time constant 88 min, and the recovery in 112 mM Ba is fitted with an exponential of time constant 17 min; neither is visible since they overlie the data points. The time constants were fitted assuming eventual recovery to 4.6 nA, the size of the current before CgTx. *B*, Recovery time constant versus Ba concentration in frog neurons; data points are mean ± SEM (n = 3–12). Test potentials were varied according to the Ba concentration as for the experiments in Figure 7. The interpulse interval was constant at 10 sec. Recovery was fitted assuming eventual recovery to the magnitude of current before CgTx block. External solutions (in mM): 5–30 $BaCl_2$, 160 TEA-Cl, 0.1 EGTA, 10 HEPES, pH 7.4 with TEA-OH; or 110 $BaCl_2$, 0.1 EGTA, 10 HEPES, pH 7.4 with $Ba(OH)_2$ (about 2 mM). *C*, Partial recovery from block by 30 μM CgTx in a rat neuron studied with 112 mM Ba. The onset of block could be fitted by a time constant of 13 sec, and the recovery was fitted with time constants of 20 min, fitted assuming partial recovery to 0.7 nA, or 40 min, fitted assuming eventual complete recovery. These on and off rate constants correspond to a K_d of 0.2–0.4 μM in 112 mM Ba.

tion. An especially interesting possibility is that the effect occurs primarily because of a competitive interaction between CgTx and divalent ions at binding sites that form part of the permeation pathway through the pore. Taken together, our results are consistent with this hypothesis, but other possibilities cannot be ruled out.

Part of the effect of increasing Ba concentrations is likely exerted relatively indirectly, as a result of screening of surface charge on the channel or membrane. We found that the blocking kinetics of CgTx could be altered dramatically without changes in Ba by changing the concentration of monovalent ions. These effects are most simply interpreted as reflecting screening of a negative surface charge. The negative surface potential from negative surface charge would produce an increase in the local concentration of the CgTx molecule, which is a basic peptide with a charge of +5 at neutral pH (Olivera et al., 1984). The effect of varying monovalent ions could be fitted well with a simple surface charge model with a surface charge of −0.004 e/Å^2 and an effective charge of CgTx of +2. The behavior of CgTx as a lower effective valence than +5 is reasonable, since only part of the molecule would be within the Debye distance over which the effects of surface charge would decay, and the CgTx molecule would certainly not behave as a simple point charge. Only charged residues near the part of the CgTx molecule that binds to the channel may contribute significantly to the effective charge of the CgTx molecule, and this may be considerably less than the charge on the whole molecule.

The effects of changing $BaCl_2$ with TEA-Cl at 160 mM were far larger than would be predicted by the simple surface charge model that could fit the effects of monovalent changes. This was especially obvious for lower Ba concentrations (for changing $BaCl_2$ from 0.5 to 2 mM, the blocking rate constant slowed by threefold), where the changes expected from surface charge screening alone are minor (10% predicted for the simple surface charge model) in the face of the effects of the constant 160 mM TEA-Cl.

On a log–log plot, the effective rate constant for CgTx blocking varied with Ba with a slope of about −1 (Fig. 7). This is what would be expected if CgTx competed with Ba for a binding site with a high affinity for Ba. The selectivity of Ca channels for divalent ions is thought to derive from high-affinity binding sites (Almers and McCleskey, 1985; Hess and Tsien, 1985), which are located at or near the external mouth of the channel (Kuo and Hess, 1993a,b). Thus, it is reasonable to hypothesize that the interaction of CgTx and Ba occurs at these same binding sites. In this case, CgTx might block the channel by the simple mechanism of physically plugging the permeation pathway. However, the results with Cd are not consistent with a model of a single binding site that can be occupied competitively by Ba, Cd, or CgTx, since the occupancy of a large fraction of channels at any one time by 1 μM Cd (which would be expected to bind and unbind fast on the time scale of CgTx binding) should then slow the overall rate of block by CgTx. The fact that CgTx block was not slowed by 1 μM Cd (which blocked by ~75%) suggests that channels with a Cd in the binding site can still be blocked by CgTx. One possibility is that Ba and Cd

←

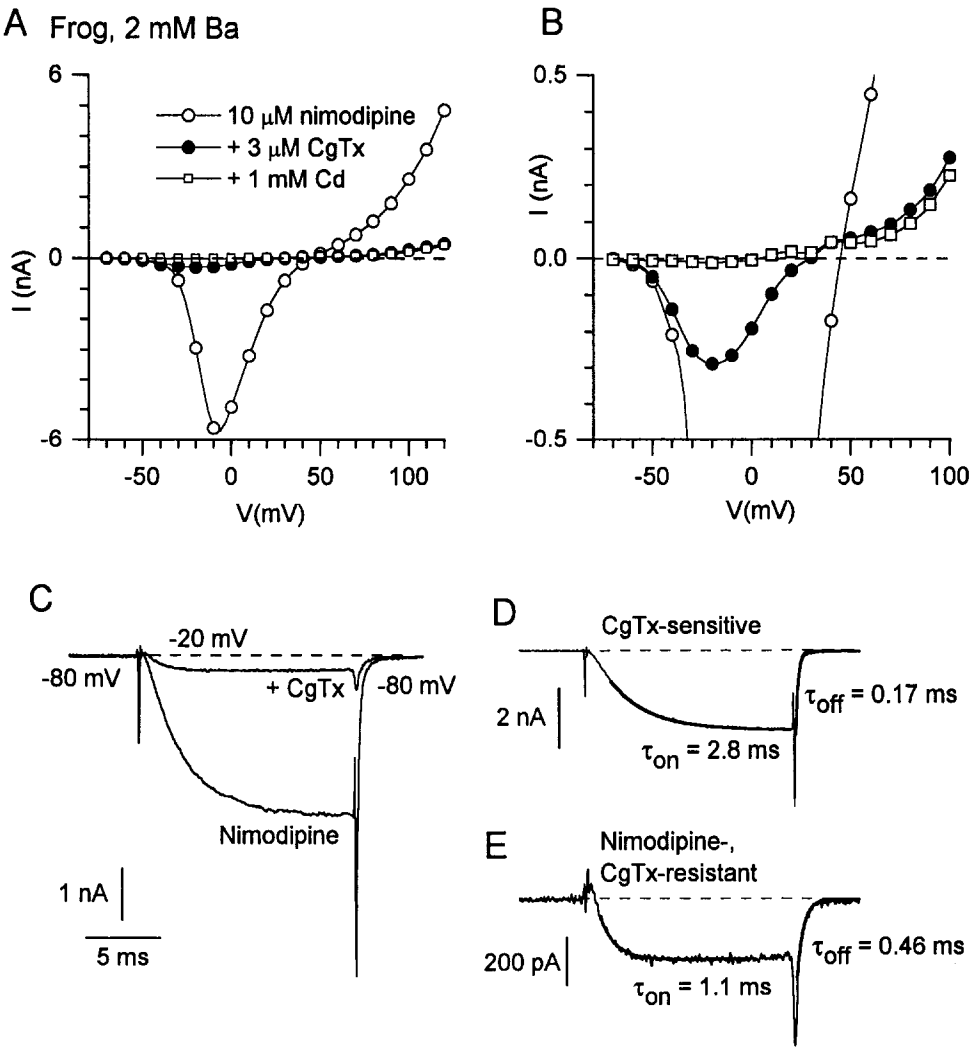

Figure 11. Current resistant to CgTx and nimodipine in a frog sympathetic neuron. CgTx (3 μM) was applied in a solution of 2 mM Ba, 160 mM TEA-Cl, 3 μM nimodipine, 3 μM TTX, 10 mμM HEPES (pH 7.4 with TEA-OH). *A*, Current–voltage relation for peak leak-corrected current in control (*open circles*), after maximal block by 3 μM CgTx (*solid circles*) and after addition of 1 mM $CdCl_2$ (*open squares*). *B*, The same points plotted with a different current scale. *C–E*, Kinetics of leak-corrected currents elicited by a step to −20 mV. In *D* and *E*, activation and deactivation phases are overlaid with single-exponential fits with the indicated time constants. Cell BC34F.

interact differently with the high-affinity binding site and that CgTx can bind when Cd is bound but not when Ba is bound.

Although the effect of Ba on blocking kinetics can be rationalized on the basis of competition for binding sites in the permeation pathway, it is also possible that the CgTx binding site is distant from the pore of the channel. CgTx might block the channel by an "allosteric" mechanism of preventing the channel from opening. In this case, the interaction between Ba and CgTx block would be mediated through binding sites for Ba distinct from the permeation pathway. The existence of such binding sites would not be surprising. In most cases, where the effects of divalent ions in shifting channel gating have been studied, models that include specific binding sites for divalents fit the data much better than simple surface charge models. This is true for effects on the gating of Na channels as well as Ca channels, so that such binding sites need have no connection with the permeation pathway of the channel.

The hypothesis that CgTx binds at the high-affinity binding sites for divalent ions in the permeating pathway can be tested by mutagenesis. The N-type Ca channel has been cloned from both human and rat brain (Dubel et al., 1992; Williams et al., 1992b; Fujita et al., 1993). For L-type channels, mutagenesis experiments have identified particular glutamate residues that help form the high-affinity binding sites involved in divalent ion permeation (Kim et al., 1993; Yang et al., 1993). It will be interesting to see if mutation of corresponding residues of N-type channels alters CgTx binding as well as ion selectivity.

Current resistant to CgTx and nimodipine

In both frog and rat sympathetic neurons, there was often significant current remaining when high concentrations of CgTx were applied in the presence of nimodipine. In frog cells, this CgTx- and dihydropyridine-resistant current generally amounted to only a few percent of the overall current when studied with low (0.5–5 mM) Ba concentrations but was much more prominent when studied with high (20–112 mM) Ba concentrations (Fig. 12). In some rat neurons studied with 5 mM Ba, there was no current remaining in CgTx and nimodipine, while in others the CgTx- and dihydropyridine-resistant current amounted to 15–20% of the overall current. The current was more regularly prominent in rat neurons studied with higher Ba concentrations.

In both frog and rat neurons, the current resistant to nimodipine and CgTx had different kinetics and voltage dependence than the predominant CgTx-sensitive current. The CgTx- and dihydropyridine-resistant current activated over a more negative voltage range, activated more rapidly, inactivated more rapidly, and had slightly slower tail currents. The differences

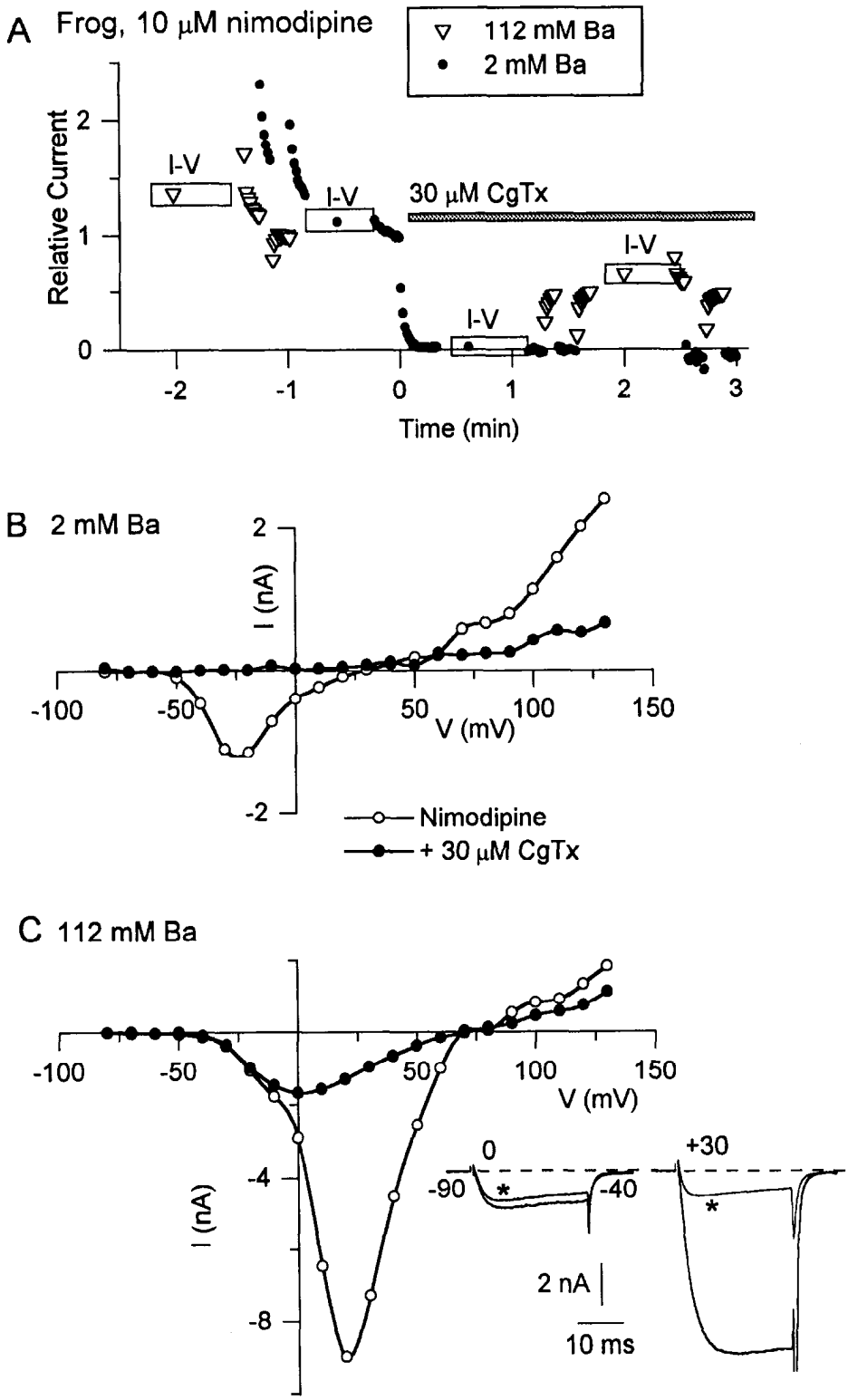

Figure 12. CgTx- and nimodipine-resistant current carried by 112 mM Ba in a frog neuron. *A*, Time course of Ba current elicited by a step to 0 mV during changes in Ba concentration and application of 30 μM CgTx. Symbols show leak-corrected current at 0 mV recorded in an external solution of 2 mM $BaCl_2$, 160 mM TEA-Cl, 10 μM nimodipine, 3 μM TTX, 10 mM HEPES (pH 7.4 with TEA-OH) (*solid circles*) or 110 mM $BaCl_2$, 10 μM nimodipine, 3 μM TTX, 10 mM HEPES, pH 7.4 with $Ba(OH)_2$ (*open inverted triangles*). Application of 30 μM CgTx in 2 mM Ba completely blocked the current, but substantial current carried by 112 Ba remained unblocked. Current was elicited every 1 sec during transitions between solutions. With CgTx, current disappeared in less than a second on switching from 112 mM Ba to 2 mM Ba while current grew for several seconds when switching from 2 mM Ba to 112 mM Ba. *B* and *C*, Current–voltage relationships with 2 mM Ba and 112 mM Ba, recorded at times indicated by *rectangles in A*. *C inset*, Leak-corrected currents elicited by steps to 0 or +30 mV before and after (*asterisk*) application of 30 μM CgTx in 112 mM Ba. Cell BC31G.

suggest that the CgTx- and dihydropyridine-resistant current arises from different channels rather than representing "CgTx-resistant N-type channels" or partial block of individual N-type channels. The CgTx- and dihydropyridine-resistant current is not like conventional T-type current, which inactivates considerably faster, activates over a more negative voltage range, and has much slower tail currents. The CgTx- and dihydropyridine-resistant current almost certainly does not represent P-type Ca channels, because previous studies have shown no effect of the P-type Ca channel blocker ω-Aga-IVA on overall current in sympathetic neurons (Mintz et al., 1992; Mintz and Bean, 1993; Zhu and Ikeda, 1993). Consistent with this, in one rat sympathetic neuron with a sizeable CgTx- and dihydropyridine-resistant current, 200 nM ω-Aga-IVA did not affect current remaining in 3 μM nimodipine and 3 μM CgTx.

Recent experiments by K. S. Elmslie, P. J. Kammermeier,

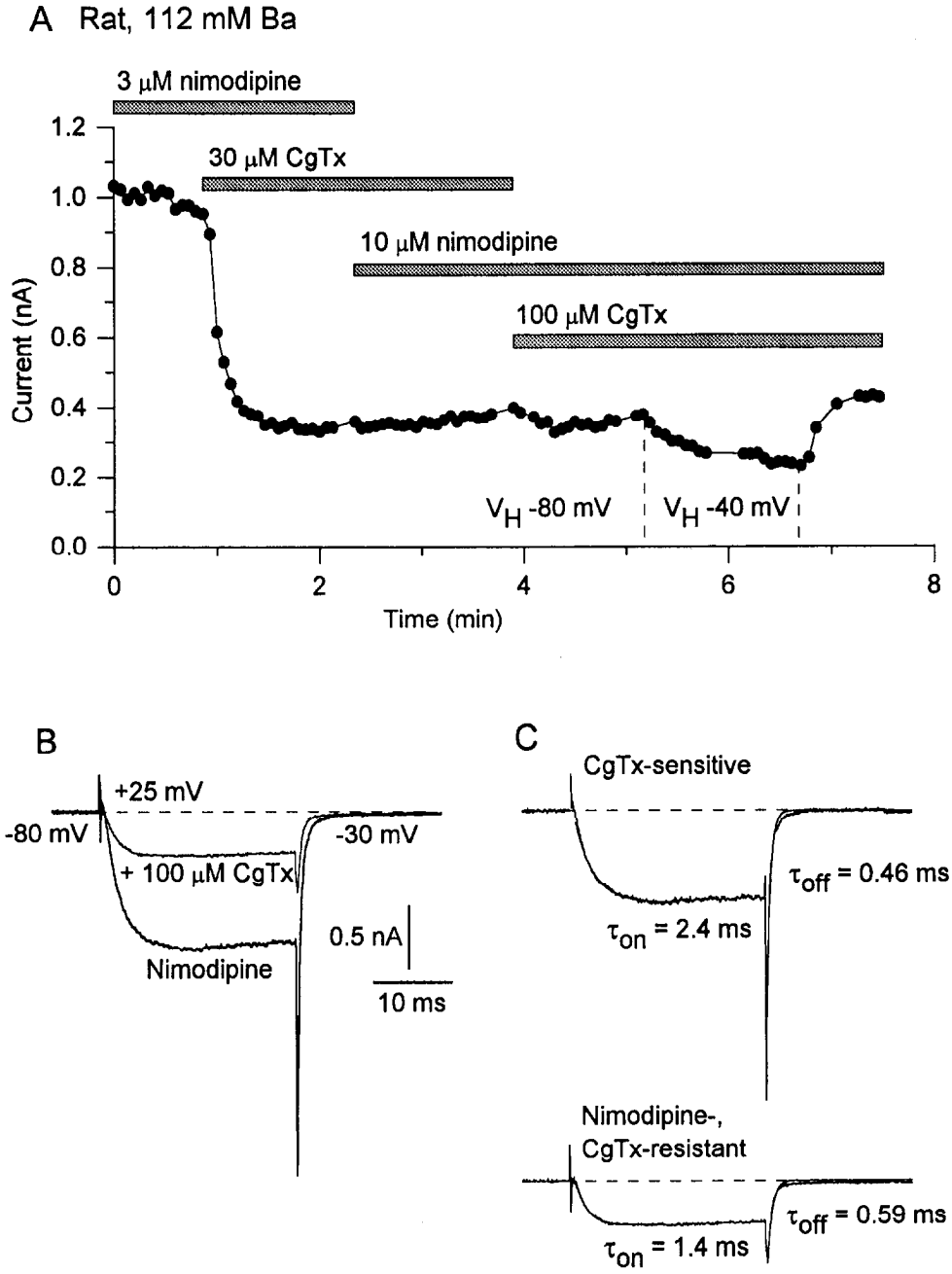

Figure 13. Current resistant to CgTx and nimodipine in a rat sympathetic neuron. *A*, Time course of the experimental protocol indicating the drug applications. The test potential was +25 mV. The holding potential was −80 mV or −40 mV, as indicated. *B*, In a different rat sympathetic neuron, leak-corrected currents elicited by a step to +25 mV before and after application of 100 μM CgTx in a solution containing 10 μM nimodipine. *C*, Kinetic comparison of CgTx-sensitive current (obtained by subtraction of the currents in *B*) and current resistant to both CgTx and nimodipine. Activation and deactivation phases are overlaid with single-exponential fits with the indicated time constants. External solution for both experiments: 110 mM $BaCl_2$, 10 mM HEPES, 3 μM TTX, pH adjusted to 7.4 with $Ba(OH)_2$.

and S. W. Jones (personal communication) have also shown in frog sympathetic neurons a prominent component of current in high Ba concentrations that is insensitive to CgTx and dihydropyridines, and they have further shown that this current is insensitive to modulation by norepinephrine, another difference from N-type channels in the neurons. It will be interesting to compare the single-channel characteristics of the CgTx- and dihydropyridine-resistant channels with N-type Ca channels. In a single-channel study on frog sympathetic neurons, Delcour et al. (1992) briefly noted the occurrence of a population of single-channel events with single-channel size smaller than normal N-type channels. They noticed that these events activated over a somewhat more negative voltage range, which would be consistent with the CgTx- and dihydropyridine-resistant current at the whole-cell level. Further correlations between whole-cell and single-channel recordings are needed.

In rat neurons, we observed considerable cell-to-cell variability in the amount of CgTx- and dihydropyridine-resistant current, and such variability is also evident in previous reports. In previous studies from our laboratory, only 5% (Regan et al., 1991) or 2% (Mintz et al., 1992) of the current in rat superior cervical ganglion neurons remained unblocked by CgTx and dihydropyridines, while 10% of the current remained in the cells studied with 300 nM CgTx (a saturating concentration) in Figure 2. It is possible that the CgTx- and dihydropyridine-resistant current is more prominent in SCG neurons from older rats, since the fraction of current blocked by CgTx is consistently smaller in neurons from adult rats (Ikeda, 1991, 1992; Zhu and Ikeda, 1993) than in younger rats (Regan et al., 1991; Mintz et al., 1992).

The characteristics of the CgTx- and dihydropyridine-resistant current do not fit neatly with those of T-type, L-type, N-type,

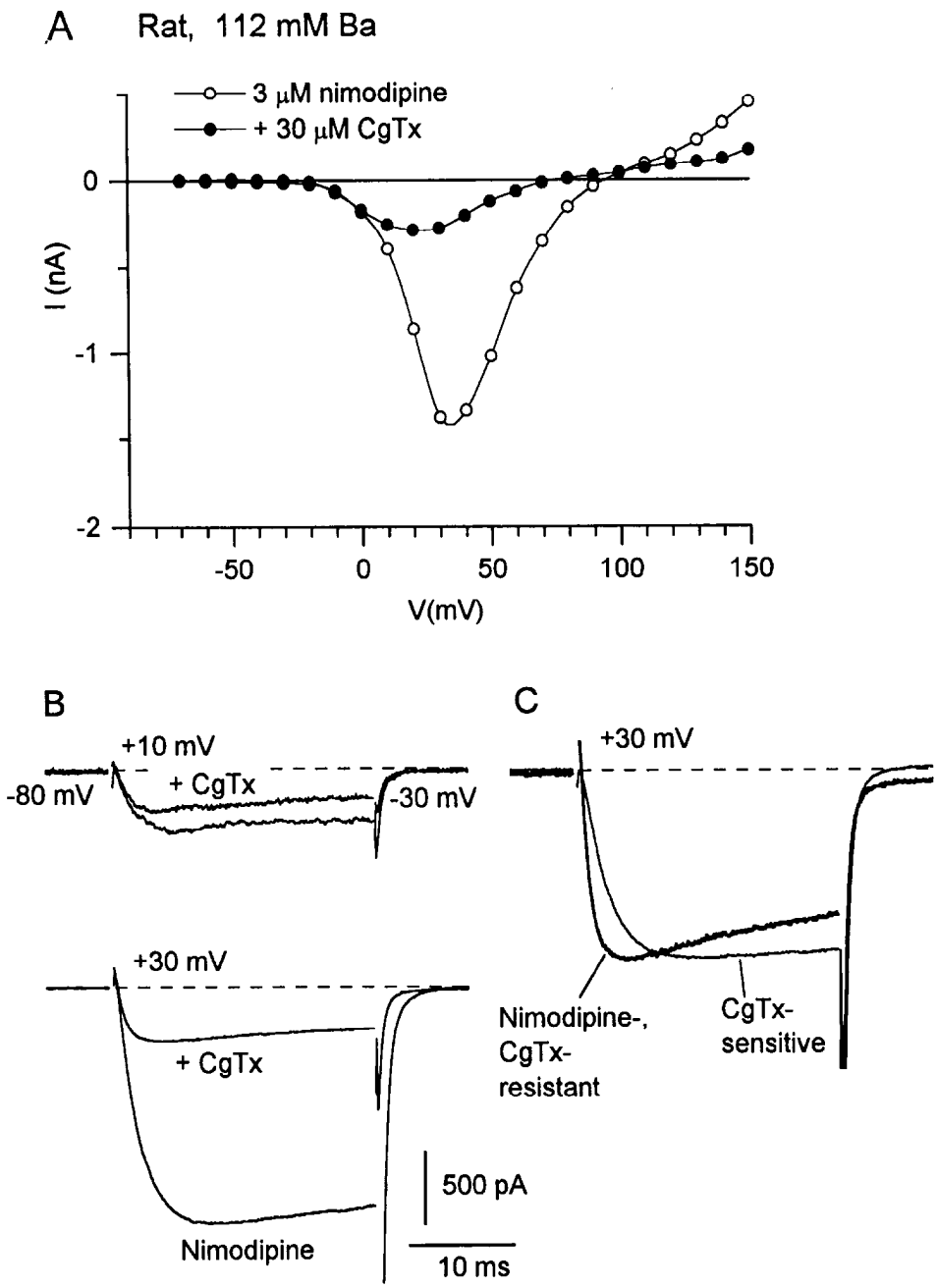

Figure 14. Current–voltage relation for CgTx- and nimodipine-resistant current in a rat neuron. CgTx (30 μM) was applied in a solution containing 110 mM $BaCl_2$, 3 μM nimodipine, 3 μM TTX, 10 mM HEPES [pH adjusted to 7.4 with $Ba(OH)_2$]. *A*, Peak current versus voltage before and after application of CgTx. *B*, Currents at +10 mV (*top*) and +30 mV (*bottom*) before and after application of CgTx. The currents at +30 mV were averaged from 10 sweeps to reduce noise. The tail current without CgTx is truncated to save space. *C*, Kinetic comparison of CgTx- and nimodipine-resistant current with CgTx-sensitive current (obtained from subtracting the traces in *B*). The currents were scaled to have the same peak magnitude. Cell LD41C.

or P-type channels. Interestingly, the characteristics (activation range lower than N- and L-type channel but higher than T-type channels, inactivation faster than N-type channels but slower than T-type channels, insensitivity to dihydropyridines, CgTx, and ω-Aga-IVA) are similar to those of two recently expressed cloned channels (Ellinor et al., 1993; Soong et al., 1993) that also do not fall neatly into existing classifications and are also reminiscent of a fraction of current in cerebellar granule neurons remaining with dihydropyridines, CgTx, and ω-conotoxin MVIIC (Ellinor et al., 1993). Many other central and peripheral neurons possess sizeable current remaining unblocked by CgTx, dihydropyridines, and ω-Aga-IVA (Mintz et al., 1992), but in most cases, the kinetics and voltage dependence of the current have not yet been characterized. Adrenal chromaffin cells (Artalejo et al., 1992) and rat insulinoma cells (Pollo et al., 1993) both possess a CgTx- and dihydropyridine-resistant current (in addition to separate components sensitive to CgTx and dihydropyridines); in adrenal chromaffin cells, the resistant current activates with somewhat faster kinetics than the CgTx-sensitive current (Artalejo et al., 1992), as we found.

An interesting unanswered question is why the CgTx- and dihydropyridine-resistant current is so much more prominent in high Ba concentrations. This is especially true in frog sympathetic cells, where in most neurons the current is almost undetectable with 2–5 mM Ba but is quite prominent with 112 mM Ba, even in the same neurons (e.g., Fig. 12). The difference may reflect resting inactivation of the channels in low Ba concentrations, which would be consistent with the current taking a few seconds to increase on fast solution changes from 2 mM to 112 mM Ba (Fig. 12). Another possibility is that the characteristics

of Ba permeation are different than L-type or N-type channels, where single-channel current increases sublinearly with Ba concentration.

References

Abe T, Koyano K, Saisu H, Nishiuchi Y, Sakakibara S (1986) Binding of ω-conotoxin to receptor sites associated with the voltage-sensitive calcium channel. Neurosci Lett 71:203–208.

Almers W, McCleskey EW (1984) Non-selective conductance in calcium channels of frog muscle: calcium selectivity in a single-file pore. J Physiol (Lond) 353:585–608.

Aosaki T, Kasai H (1989) Characterization of two kinds of high-voltage-activated Ca channel currents in chick sensory neurons: different sensitivity to dihydropyridines and ω-conotoxin GVIA. Pfluegers Arch 414:150–156.

Artalejo CR, Perlman RL, Fox AP (1992) Omega-conotoxin GVIA blocks a Ca^{2+} current in bovine chromaffin cells that is not of the "classic" N type. Neuron 8:85–95.

Barhanin J, Schmid A, Lazdunski M (1988) Properties of structure and interaction of the receptor for ω-conotoxin, a polypeptide active on Ca^{2+} channels. Biochem Biophys Res Commun 150:1051–1062.

Bean, BP (1989) Classes of calcium channels in vertebrate cells. Annu Rev Physiol 51:367–384.

Bernheim L, Beech DJ, Hille B (1991) A diffusible second messenger mediates one of the pathways coupling receptors to calcium channels in rat sympathetic neurons. Neuron 6:859–867.

Boland LM, Bean BP (1993) Modulation of N-type calcium channels in bullfrog sympathetic neurons by luteinizing hormone releasing hormone: kinetics and voltage-dependence. J Neurosci 13:516–533.

Cox DH, Dunlap K (1992) Pharmacological discrimination of N-type from L-type calcium current and its selective modulation by transmitters. J Neurosci 12:906–914.

Cruz LJ, Olivera BM (1986) Calcium channel antagonists. Omega-conotoxin defines a new high-affinity site. J Biol Chem 261:6230–6233.

Dubel SJ, Starr TB, Hell J, Ahlijanian MK, Enyeart JJ, Catterall WA, Snutch TP (1992) Molecular cloning of the α-1 subunit of an ω-conotoxin-sensitive calcium channel. Proc Natl Acad Sci USA 89:5058–5062.

Ellinor PT, Zhang J-F, Randall AD, Zhou M, Schwarz TL, Tsien RW, Horne WA (1993) Functional expression of a rapidly inactivating neuronal calcium channel. Nature 363:455–458.

Feigenbaum P, Garcia ML, Kaczorowski GJ (1988) Evidence for distinct sites coupled to high affinity omega-conotoxin receptors in rat brain synaptic plasma membrane vesicles. Biochem Biophys Res Commun 154:298–305.

Feldman DH, Olivera BM, Yoshikami D (1987) Omega *Conus geographus* toxin: a peptide that blocks calcium channels. FEBS Lett 214: 295–300.

Forscher P, Oxford GS (1985) Modulation of calcium channels by norepinephrine in internally dialyzed avian sensory neurons. J Gen Physiol 85:743–763.

Fox AP, Nowycky MC, Tsien RW (1987) Kinetic and pharmacologic properties distinguishing three types of calcium currents in chick sensory neurones. J Physiol (Lond) 94:149–172.

Fujita Y, Mynlieff M, Dirksen RT, Kim M-S, Niidome T, Nakai J, Friedrich T, Iwabe N, Miyata T, Furuichi T, Furutama D, Mikoshiba K, Mori Y, Beam KG (1993) Primary structure and functional expression of the ω-conotoxin-sensitive N-type calcium channel from rat brain. Neuron 10:585–598.

Hamill OP, Marty A, Neher E, Sakmann B, Sigworth FJ (1981) Improved patch-clamp techniques for high-resolution current recording from cells and cell-free membrane patches. Pfluegers Arch 391:85–100.

Hess P (1990) Calcium channels in vertebrate cells. Annu Rev Neurosci 13:337–356.

Hess P, Tsien RW (1984) Mechanism of ion permeation through calcium channels. Nature 309:453–456.

Hess P, Lansman JB, Tsien RW (1984) Different modes of Ca channel gating behavior favored by dihydropyridine Ca agonists and antagonists. Nature 311:538–544.

Hille B (1992) Ionic channels of excitable membrane. Sunderland, MA: Sinauer.

Hirning LD, Fox AP, McCleskey EW, Olivera BM, Thayer SA, Miller RJ, Tsien RW (1988) Dominant role of N-type Ca^{2+} channels in evoked release of norepinephrine from sympathetic neurons. Science 239:57–61.

Ikeda SR (1991) Double-pulse calcium channel facilitation in adult rat sympathetic neurons. J Physiol (Lond) 439:181–214.

Ikeda SR (1992) Prostaglandin modulation of Ca^{2+} channels in rat sympathetic neurones is mediated by guanine nucleotide binding proteins. J Physiol (Lond) 458:339–359.

Jones SW, Jacobs (1990) Dihydropyridine actions on calcium currents of frog sympathetic neurons. J Neurosci 10:2261–2267.

Jones SW, Marks TN (1989) Calcium currents in bullfrog sympathetic neurons. I. Activation kinetics and pharmacology. J Gen Physiol 94: 151–167.

Kasai H, Neher E (1992) Dihydropyridine-sensitive and ω-conotoxin sensitive calcium channels in a mammalian neuroblastoma-glioma cell line. J Physiol (Lond) 448:161–188.

Kasai H, Aosaki T, Fukada J (1987) Presynaptic Ca-antagonist ω-conotoxin irreversibly blocks N-type Ca channels in chick sensory neurons. Neurosci Res 4:228–235.

Kim M-K, Mori T, Sun L-X, Imoto K, Mori Y (1993) Structural determinants of ion selectivity in brain calcium channel. FEBS Lett 318:145–148.

Kuo C-C, Hess P (1993a) Ion permeation through the L-type Ca^{2+} channel in rat phaeochromocytoma cells: two sets of ion binding sites in the pore. J Physiol (Lond) 466:629–655.

Kuo C-C, Hess P (1993b) Characterization of the high-affinity Ca^{2+} binding sites in the L-type Ca^{2+} channel pore in rat phaeochromocytoma cells. J Physiol (Lond) 466:657–682.

McCleskey EW, Fox AP, Feldman DH, Cruz LJ, Olivera BM, Tsien RW, Yoshikami D (1987) ω-Conotoxin: direct and persistent blockade of specific types of calcium channels in neurons but not muscle. Proc Natl Acad Sci USA 84:4327–4331.

Mintz IM, Bean BP (1993) Block of calcium channels in rat neurons by synthetic ω-Aga-IVA. Neuropharmacology 32:1161–1169.

Mintz IM, Adams ME, Bean BP (1992) P-type calcium channels in central and peripheral neurons. Neuron 9:1–20.

Mynlieff M, Beam KG (1992) Characterization of voltage-dependent calcium currents in mouse motoneurons. J Neurophysiol 68:85–92.

Nowycky MC, Fox AP, Tsien RW (1985) Three types of neuronal calcium channel with different calcium agonist sensitivity. Nature 316:440–443.

Olivera BM, McIntosh JM, Cruz LJ, Luque FA, Gray WR (1984) Purification and sequence of a presynaptic peptide toxin from *Conus geographus* venom. Biochemistry 23:5087–5090.

Plummer MR, Logothetis DE, Hess P (1989) Elementary properties and modulation of calcium channels in mammalian peripheral neurons. Neuron 2:1453–1463.

Pollo A, Lovallo M, Biancardi E, Sher E, Socci C, Carbone E (1993) Sensitivity to dihydropyridines, ω-conotoxin, and noradrenaline reveals multiple high-voltage-activated Ca^{2+} channels in rat insulinoma and human pancreatin b-cells. Pfluegers Arch 423:462–471.

Regan LJ, Sah DWY, Bean BP (1991) Ca^{2+} channels in rat central and peripheral neurons: high-threshold current resistant to dihydropyridine blockers and ω-conotoxin. Neuron 6:269–280.

Sigworth F (1980) The variance of sodium current fluctuations at the node of Ranvier. J Physiol (Lond) 307:97–129.

Soong TW, Stea A, Hodson CD, Dubel SJ, Vincent SR, Snutch TP (1993) Structure and functional expression of a member of the low voltage-activated calcium channel family. Science 260:1133–1136.

Wagner JA, Snowman MA, Biswas A, Olivera BM, Snyder SH (1988) ω-Conotoxin GVIA binding to a high-affinity receptor in brain: characterization, calcium sensitivity, and solubilization. J Neurosci 8:3354–3359.

Williams ME, Feldman DH, McCue AF, Brenner R, Velicelebi G, Ellis SB, Harpold MM (1992a) Structure and function of a1, a2, and b subunits of a novel human neuronal calcium channel subtype. Neuron 8:71–84.

Williams ME, Brust PF, Feldman DH, Saraswathi P, Simerson S, Maoufi A, McCue AF, Velicelebi G, Ellis SB, Harpold MM (1992b) Structure and functional expression of an ω-conotoxin-sensitive human N-type calcium channel. Science 257:389–395.

Yang J, Ellinor PT, Sather WA, Zhang J-F, Tsien RW (1993) Molecular determinants of Ca^{2+} selectivity and ion permeation in L-type Ca^{2+} channels. Nature, in press.

Zhu Y, Ikeda SR (1993) Adenosine modulates voltage-gated Ca^{2+} channels in adult rat sympathetic neurons. J Neurophysiol 70:610–620.